Calcium and electrical dynamics in lymphatic endothelium

Erik J. Behringer[1,2], Joshua P. Scallan[2,3], Mohammad Jafarnejad[4], Jorge A. Castorena-Gonzalez[2], Scott D. Zawieja[2], James E. Moore Jr[4], Michael J. Davis[2,5] and Steven S. Segal[2,5]

[1] *Basic Sciences, Loma Linda University, Loma Linda, CA 92350, USA*
[2] *Department of Medical Pharmacology and Physiology, University of Missouri, Columbia, MO 65212, USA*
[3] *Department of Molecular Pharmacology and Physiology, University of South Florida, Tampa, FL 33612, USA*
[4] *Department of Bioengineering, Imperial College London, London, England*
[5] *Dalton Cardiovascular Research Center, Columbia, MO, 65211, USA*

Edited by: Kim Barrett & Kathleen Morgan

The Journal of Physiology

Key points

- Endothelial cell function in resistance arteries integrates Ca^{2+} signalling with hyperpolarization to promote relaxation of smooth muscle cells and increase tissue blood flow. Whether complementary signalling occurs in lymphatic endothelium is unknown.
- Intracellular calcium and membrane potential were evaluated in endothelial cell tubes freshly isolated from mouse collecting lymphatic vessels of the popliteal fossa. Resting membrane potential measured using intracellular microelectrodes averaged ~ -70 mV.
- Stimulation of lymphatic endothelium by acetylcholine or a TRPV4 channel agonist increased intracellular Ca^{2+} with robust depolarization. Findings from $Trpv4^{-/-}$ mice and with computational modelling suggest that the initial mobilization of intracellular Ca^{2+} leads to influx of Ca^{2+} and Na^+ through TRPV4 channels to evoke depolarization.
- Lymphatic endothelial cells lack the Ca^{2+}-activated K^+ channels present in arterial endothelium to generate endothelium-derived hyperpolarization. Absence of this signalling pathway with effective depolarization may promote rapid conduction of contraction along lymphatic muscle during lymph propulsion.

Abstract Subsequent to a rise in intracellular Ca^{2+} ($[Ca^{2+}]_i$), hyperpolarization of the endothelium coordinates vascular smooth muscle relaxation along resistance arteries during blood flow control. In the lymphatic vasculature, collecting vessels generate rapid contractions coordinated along lymphangions to propel lymph, but the underlying signalling pathways are unknown. We tested the hypothesis that lymphatic endothelial cells (LECs) exhibit Ca^{2+} and electrical signalling properties that facilitate lymph propulsion. To study electrical and intracellular Ca^{2+} signalling dynamics in lymphatic endothelium, we excised collecting lymphatic vessels from the popliteal fossa of mice and removed their muscle cells to isolate intact LEC tubes (LECTs). Intracellular recording revealed a resting membrane potential of ~ -70 mV. Acetylcholine (ACh) increased $[Ca^{2+}]_i$ with a time course similar to that observed in endothelium of resistance arteries (i.e. rapid initial peak with a sustained 'plateau'). In striking contrast to the endothelium-derived hyperpolarization (EDH) characteristic of arteries, LECs depolarized (>15 mV) to either ACh or TRPV4 channel activation. This depolarization was facilitated by the absence of Ca^{2+}-activated K^+ (K_{Ca}) channels as confirmed with PCR, persisted in the absence of extracellular Ca^{2+}, was abolished by $LaCl_3$ and was attenuated $\sim 70\%$ in LECTs from $Trpv4^{-/-}$ mice. Computational modelling of ion fluxes in LECs indicated that omitting K^+ channels supports our experimental results. These

---

E. J. Behringer and J. P. Scallan contributed equally to this work.

findings reveal novel signalling events in LECs, which are devoid of the K_{Ca} activity abundant in arterial endothelium. Absence of EDH with effective depolarization of LECs may promote the rapid conduction of contraction waves along lymphatic muscle during lymph propulsion.

Corresponding authors M. J. Davis and S. S. Segal: Department of Medical Pharmacology and Physiology, 1 Hospital Drive, MA415 Medical Science Building, University of Missouri, Columbia, MO 65212, USA. Email: davismj@health.missouri.edu and segalss@health.missouri.edu

Abbreviations ACh, acetylcholine; AECT, arterial endothelial cell tube (popliteal); $[Ca^{2+}]_i$, intracellular Ca^{2+} concentration; $[Ca^{2+}]_o$, extracellular Ca^{2+} concentration; $[Ca^{2+}]_{IS}$, Ca^{2+} concentration in IP_3-sensitive store; CaCC, Ca^{2+}-activated Cl^- channel; BK_{Ca}, large-conductance Ca^{2+}-activated K^+ channel; EC, endothelial cell; EDH, endothelial derived hyperpolarization; eNOS, endothelial nitric oxide synthase; ER, endoplasmic reticulum; GSK101, GSK1016790A, TRPV4 channel activator; K_{ATP}, ATP-sensitive K^+; K_{Ca}, Ca^{2+}-activated K^+; K_{IR}, inward-rectifying K^+; $[K^+]_o$, extracellular K^+ concentration; Ing-Ax, inguinal efferent-axillary afferent; IP_3, inositol 1,4,5-trisphosphate; IP_3R, inositol trisphosphate receptor; LEC, lymphatic endothelial cell; LECT, lymphatic endothelial cell tube (popliteal); LMC, lymphatic muscle cell; NaK, Na^+–K^+-ATPase; NKCC, Na^+–K^+–Cl^- cotransporter; NO, nitric oxide; PMCA, plasma membrane Ca^{2+}-ATPase; PSS, physiological salt solution; SK_{Ca}/IK_{Ca}, small- and intermediate-conductance Ca^{2+}-activated K^+ channels; SERCA, sarco(endo)plasmic reticulum Ca^{2+}-ATPase; SMC, smooth muscle cell (vascular); TRP, transient receptor potential; TRPV4, transient receptor potential vanilloid type 4; $Trpv4^{-/-}$, $Trpv4$ knockout; V_m, membrane potential; VRAC, volume-regulated anion channel; WT, wild-type.

Introduction

Endothelium-derived hyperpolarization (EDH) is integral to the control of vascular resistance, tissue blood flow and oxygen delivery (Busse *et al.* 2002; Garland & Dora, 2017). In contrast to endothelial cell (EC)-dependent signalling mediated through the release and diffusion of autacoids (e.g. nitric oxide (NO) and prostaglandins), the EDH pathway serves as a direct electrical signal that spreads through gap junctions from EC to EC and from ECs to smooth muscle cells (SMCs) to promote vasodilatation (Bagher & Segal, 2011). The longitudinal spread of hyperpolarization conforms to passive cable properties demonstrated in both intact resistance arteries containing SMCs (Emerson *et al.* 2002) and their freshly isolated endothelial cell tubes (Behringer & Segal, 2012). EDH entails an increase in cytosolic Ca^{2+} concentration ($[Ca^{2+}]_i$) that activates small- and intermediate-conductance Ca^{2+}-activated K^+ channels (SK_{Ca}/IK_{Ca}) in the plasma membrane (Félétou, 2016; Garland & Dora, 2017). As such, the initiation of EDH is a classic example of the intimate interaction between Ca^{2+} homeostasis and alterations in V_m (Busse *et al.* 1988; Behringer & Segal, 2015) and this relationship is integral to blood flow regulation throughout the body (Félétou, 2016).

Collecting lymphatic vessels perform multiple distinct physiological roles (Aspelund *et al.* 2016), including the rapid coordination of contraction and relaxation driven by lymphatic muscle cells (LMCs) to pump fluid centrally from peripheral tissues (von der Weid *et al.* 1996; Scallan & Davis, 2013; Scallan *et al.* 2013). Whereas lymphatic endothelial cell function has focused largely on the NO pathway (Chakraborty *et al.* 2015), the potential for EDH signalling in isolated endothelium of collecting lymphatics is unknown. Resolving the determinants of electrical signalling in lymphatic vessels is integral to understanding how they maintain the ability to contract rapidly to move lymph against a pressure gradient. Thus, if the EDH pathway is activated in lymphatic vessels, relaxation of LMCs may interfere with effective pumping. Indeed, lymphatic vessels isolated from mice that lack endothelial nitric oxide synthase (i.e. $eNOS^{-/-}$) do not dilate in response to the muscarinic receptor type 3 (M_3) agonist acetylcholine (ACh). Instead, they display enhanced constriction and increased contraction frequency (Scallan & Davis, 2013). The absence of residual dilatation to ACh in lymphatics from $eNOS^{-/-}$ mice suggests that LECs lack EDH signalling characteristic of blood vessels in response to SK_{Ca}/IK_{Ca} activation. If lymphatic endothelium indeed lacks signalling via the EDH pathway, it would be markedly different from endothelium studied in the context of blood flow control.

In the present study, we tested the hypothesis that LECs exhibit Ca^{2+} and electrical signalling properties that permit lymph propulsion. To investigate simultaneous $[Ca^{2+}]_i$ and electrical responses of native intact lymphatic ECs in the absence of LMC influences, LEC tubes (LECTs) were isolated from popliteal collecting lymphatic vessels of C57BL/6 mice (1–2 months old) using mild enzymatic digestion and gentle trituration. Arterial endothelial cell tubes (AECTs) isolated from popliteal arteries were studied under identical conditions as a positive control for EDH signalling in blood vessels. Sharp microelectrodes and Fura-2 photometry were used to measure membrane potential (V_m) and $[Ca^{2+}]_i$, respectively, in response to ACh, which involves the internal release of Ca^{2+}

followed by Ca^{2+} influx, or in response to the transient receptor potential vanilloid type 4 (TRPV4) agonist GSK1016790A (GSK101), which mediates Ca^{2+} influx. We found that despite the similar time course of intracellular $[Ca^{2+}]_i$ dynamics in response to ACh, LECTs depolarize instead of hyperpolarizing in the manner of AECTs, indicating the lack of an EDH pathway. Using intact pressurized lymphatic vessels, we verified that lymphatic endothelium depolarized to ACh. This finding was supported by RT-PCR demonstrating the absence of mRNA for *Kcnn3* and *Kcnn4* (which encode SK_{Ca} and IK_{Ca} proteins, respectively) in LECTs, which contrasts with their known expression in AECTs. Despite the absence of Ca^{2+}-activated K^+ (K_{Ca}) channels and their association with TRPV4 channels in blood vessels (Sonkusare *et al.* 2012, 2014), LECTs of $Trpv4^{-/-}$ mice exhibited significantly reduced responses to ACh with both $[Ca^{2+}]_i$ ($\sim$50%) and membrane depolarization ($\sim$70%) *versus* C57BL/6 controls. To gain further insight into which ion channel(s) enable depolarization in response to the rise in $[Ca^{2+}]_i$, a computational model of lymphatic endothelium was applied.

Methods

Animal care and use

All animal care and experimental procedures were approved by the Animal Care and Use Committee of the University of Missouri and performed in accord with the National Research Council's *Guide for the Care and Use of Laboratory Animals* (8th edn, 2011). Mice were housed in an enriched environment maintained on a 12:12 h light–dark cycle at $\sim$23°C with fresh tap water and standard chow available *ad libitum*. Experiments were performed on male C57BL/6 mice (1–2 months old; $n = 33$) purchased from Charles River Laboratories (Wilmington, MA, USA). In complementary experiments, male $Trpv4^{-/-}$ mice (C57BL/6 background, $n = 4$) bred at the University of Missouri (breeders obtained from GlaxoSmithKline (King of Prussia, PA, USA)) were used to investigate the role of TRPV4 (Thorneloe *et al.* 2008) in mediating $[Ca^{2+}]_i$ influx. Each mouse was anaesthetized using pentobarbital sodium (60 mg kg^{-1}, I.P. injection). Upon completion of tissue removal, the anaesthetized mouse was killed by exsanguination.

Solutions

Popliteal collecting lymphatic vessels were dissected while immersed in a Krebs buffer containing (in mM): 146.9 NaCl, 4.7 KCl, 2 $CaCl_2 \cdot 2H_2O$, 1.2 $MgSO_4$, 1.2 $NaH_2PO_4 \cdot H_2O$, 1.2 $NaHCO_3$, 1.5 Hepes, 5 D-glucose. Control physiological salt solution (PSS) was used for the dissociation procedure and all electrical and Ca^{2+} recordings, and contained the following (in mM): 140 NaCl, 5 KCl, 2 $CaCl_2$, 1 $MgCl_2$, 10 Hepes, 10 D-glucose. The pH of all solutions was adjusted to 7.4 before use. During dissociation of lymphatic or arteriolar muscle cells to obtain endothelial cell tubes, PSS contained 0.62 mg ml^{-1} papain ($\geq$6 units), 1.5 mg ml^{-1} collagenase ($\geq$15 units), 1.0 mg ml^{-1} dithioerythritol, 0.1% bovine serum albumin (USB Corp., Cleveland, OH, USA) and 0.1 mM $CaCl_2$. For experiments with nominally zero $[Ca^{2+}]_o$, $CaCl_2$ was isosmotically replaced with NaCl. Reagents were purchased from Sigma-Aldrich (St Louis, MO, USA) unless indicated otherwise.

Surgery and microdissection

Once a mouse was anaesthetized, the fur covering each hindlimb was removed by shaving. With the mouse in the prone position, a $\sim$1 cm L-shaped incision was made from the ankle towards the knee to expose the saphenous vein. While viewing through a stereomicroscope, connective tissue surrounding the saphenous vein was carefully cut to expose a superficial popliteal lymphatic vessel intimately associated with the vein. The collecting lymphatic vessel and associated adipose tissue were then carefully removed from the vein using microdissection and placed in Krebs buffer. Two popliteal collecting lymphatic vessels were removed per mouse (one per leg). In separate experiments, the popliteal artery was removed from each leg in similar fashion. Vessels were then pinned to the bottom of a chamber coated with transparent Sylgard® rubber (Dow Corning, Midland, MI, USA) before adipose and connective tissue were removed using microdissection, then vessels were transferred to a glass tube containing the dissociation buffer and enzymes. We found it unnecessary to clean lymphatic vessels completely with microdissection as performed previously (Scallan & Davis, 2013) since enzymatic digestion facilitated the removal of connective tissue.

For endothelial V_m measurements of isolated and pressurized lymphatic vessels, inguinal efferent-axillary afferent (Ing-Ax) internodal collecting vessels were used due to their amenability for removal of connective tissue, which facilitated access of the microelectrode to the endothelial layer while limiting trauma to smooth muscle and ECs. In brief, a midline dorsal incision and retraction of the skin fold revealed the large Ing-Ax paralleling the superficial epigastric vein. The Ing-Ax lymphatic vessel and surrounding connective tissue was removed by dissection and further cleaned in a Sylgard-coated dish in Krebs buffer supplemented with 0.5% BSA.

Endothelial cell tube isolation and superfusion

Popliteal AECTs and LECTs were prepared as recently described (Socha & Segal, 2013). Briefly, vessel segments

were then rinsed with PSS lacking enzymes and transferred to a tissue chamber (RC-27N, Warner Instruments, Hamden, CT, USA) containing PSS at room temperature. To dissociate muscle cells from the endothelial layer, a vessel segment was incubated with an enzyme cocktail (see 'Solutions') at 34°C for either 30 min (arteries) or 20 min (lymphatic vessels). The vessel segment was then gently triturated using aspiration and ejection from a micropipette during visual inspection at ×200. Dissociation pipettes were prepared from borosilicate glass capillary tubes (1.0 mm outer diameter (o.d.)/ 0.58 mm internal diameter (i.d.); World Precision Instruments (WPI), Sarasota, FL, USA) pulled (P-97; Sutter Instruments, Novato, CA, USA) and heat-polished at one end (tip i.d.: ∼50–70 μm). The tissue chamber containing the freshly isolated EC tube (width: ∼40 μm, length: 0.3–1 mm) was secured to an aluminium platform (width: 14.5 cm, length: 24 cm, thickness: 0.4 cm). A micromanipulator (DT3-100, Siskiyou Corp., Grants Pass, OR, USA) mounted at each end of the platform held a blunt-ended, heat-polished micropipette (o.d., 60–100 μm) used to position and secure the EC tube against the bottom (coverslip) of the tissue chamber. The aluminium platform was mounted on an inverted microscope (Eclipse TS100, Nikon) located on a vibration-isolated table (Technical Manufacturing Corp., Peabody, MA, USA) and superfused with control PSS at ∼4 ml min^{-1} along the axis of the EC tube. Throughout the experiments, temperature was maintained at 28 °C using an in-line heater (SH-27B, Warner) and heating platform (PH6, Warner) coupled to a temperature controller (TC-344B, Warner). Preparations were stable for the duration of experiments (1–2 h) under these conditions.

Ca^{2+} photometry

Ca^{2+} photometry was performed using an IonOptix system (Milford, MA, USA) as described (Socha *et al.* 2011; Behringer & Segal, 2015). Briefly, prior to loading Fura-2 dye, the preparation was maintained at room temperature for 10 min while autofluorescence was recorded at 510 nm during alternate excitation at 340 and 380 nm (10 Hz). Fura-2 AM dye (5 μM; F14185, Thermo Fisher Scientific, Waltham, MA, USA) was loaded for 20 min followed by 20 min washout to allow time for intracellular de-esterification and removal of excess dye. Temperature was raised to 28°C during the final 10 min. Autofluorescence during excitation at 340 and 380 nm (average values over 30 s acquisition) was subtracted from the respective recordings at 510 nm. Using a ×40 objective (Nikon S Fluor; numerical aperture, 0.90), the imaging window was 140 μm (length) by ∼40 μm (width) and contained ∼40–50 ECs (Behringer & Segal, 2015).

Intracellular recording of V_m

Endothelial cell tubes. Microelectrodes were pulled (P-97; Sutter) from glass capillary tubes (GC100F-10, Warner) and backfilled with 2 M KCl (tip resistance, ∼150 MΩ). Membrane potential was measured using Axoclamp 2B (Molecular Devices, Sunnyvale, CA, USA) and Warner IE-210 electrometers as described (Behringer & Segal, 2012; Behringer *et al.* 2012). An Ag/AgCl pellet placed in effluent PSS served as a reference electrode. Amplifier outputs were connected to an analog-to-digital converter (Digidata 1322A, Molecular Devices) and data were recorded at 1000 Hz on a Dell personal computer using Axoscope 10.1 software (Molecular Devices). Individual cells were impaled along the midline of the EC tube while viewing at ×400 magnification. For lymphatic endothelium, successful impalements were indicated by a sharp negative deflection of V_m and typically required ∼5 min for stabilization to resting V_m (approx. range: −50 to −80 mV) before applying pharmacological agents. For AECTs, V_m typically stabilized within 1 min (resting V_m range: −25 to −40 mV) following impalement (Behringer & Segal, 2012, 2015 Behringer *et al.* 2012). For simultaneous Ca^{2+} photometry and electrophysiology, the photometric window for acquiring Ca^{2+} measurements was positioned adjacent to the electrode recording V_m (Behringer & Segal, 2015).

Intact Ing-Ax lymphatic vessels. The vessel was cannulated on glass pipettes (∼80 μm) in an observation chamber with a Burg-style V-track mounting system and transferred to an inverted microscope (Zeiss, model IM35). Both pipettes were attached to a single pressure reservoir with an output line that was split with a T-connector. Pressure was set to 8 cmH$_2$O and the vessel was lengthened to remove axial slack. Afterward, pressure was set to 3 cmH$_2$O for the duration of the experiment. A peristaltic pump constantly exchanged the Krebs buffer in the observation chamber with fresh buffer at 0.5 ml min^{-1}. A heat exchanger connected to the water-jacketed observation chamber warmed the vessel to 37°C over 30–60 min. Spontaneous contractions typically began within 10 min and stabilized by 30 min. Wortmannin (2 μM) was then added to minimize, but not completely abolish, contraction amplitude to prevent dislodging the recording electrode. Membrane potential in the endothelium was recorded using intracellular microelectrodes (250–300 MΩ) filled with 1 M KCl and advanced through the smooth muscle layer. Impalements of LECs were confirmed by the lack of action potentials (an indicator of the electrical activity of adjacent smooth muscle cells) and resting V_m ∼ −70 mV (Von der Weid & Van Helden, 1997). Membrane potential was sampled at 1 kHz using a NPI SEC-05X amplifier (ALA instruments, Farmingdale, NY, USA) and acquired on a

Table 1. Primer sets used for RT-PCR

Protein	Gene	Strand	Sequence	Accession no.	Amplicon
SK3	*Kcnn3*	S	GAC CGA ACT GTC TTG GGG TT	NM_080466	294
		AS	GCC CGA GAT GGG GTA TAG GA		
IK	*Kcnn4*	S	GAC ATC AGC GCA AGA TGC TG	NM_008433	290
		AS	CTT CTG TGA GTT CAT GTG GAG C		
α-Actin	*Acta2*	S	GTG AAG AGG AAG ACA GCA CAG	NM_007392	146
		AS	GCC CAT TCC AAC CAT TAC TCC		
VE-cadherin	*Cdh5*	S	CTT CCT TAC TGC CCT CAT TGT	NM_009868	313
		AS	CTG TTT CTC TCG GTC CAA GTT		

personal computer using a custom (Davis *et al.* 2012) LabVIEW program (National Instruments, Austin, TX, USA). Once impaled, membrane potential was allowed to stabilize over a period of a 2 min before ACh was applied. Upon completion of recording, the microelectrode was retracted and V_m values were adjusted, if appropriate, based on the offset potential (typically ≤ 5 mV).

Pharmacology

Acetylcholine (ACh; 1 μM) was used to activate G_q protein-coupled signalling through muscarinic receptors, which, in arteriolar ECs, activates Ca^{2+} release through IP_3 receptors and Ca^{2+} influx via transient receptor potential (TRP) channels (Busse *et al.* 2002). The TRPV4 agonist GSK1016790A (GSK101; 10–100 nM) was used to stimulate Ca^{2+} influx and thereby elevate $[Ca^{2+}]_i$. GSK101 was applied only once to each experimental preparation. Complementary experiments were performed using LECTs isolated from $Trpv4^{-/-}$ mice in which the gene encoding TRPV4 was deleted (Thorneloe *et al.* 2008).

Other pharmacological agents included $LaCl_3$ (100 μM; non-selective cation channel blocker), $BaCl_2$ (100 μM; K_{IR} channel blocker), NS309 (10 μM; SK_{Ca}/IK_{Ca} activator; Tocris Bioscience, Bristol, UK), apamin (300 nM; SK_{Ca} blocker; Anaspec, Fremont, CA, USA) + charbydotoxin (100 nM; IK_{Ca} and BK_{Ca} blocker; Anaspec), paxilline (1 μM; BK_{Ca} blocker; Tocris), levcromakalim (10 μM; K_{ATP} channel opener; Tocris) and glyburide (10 μM; K_{ATP} channel blocker; Tocris). A maximal concentration of 0.1% DMSO was applied to any given preparation and vehicle controls were performed to confirm that $[Ca^{2+}]_i$ and V_m were unaffected by this concentration of DMSO.

Endpoint RT-PCR

After validating the primers (Table 1), EC tubes were isolated from an artery and from a lymphatic vessel of the popliteal fossa as described above. RNA expression for

the *Kcnn3* and *Kcnn4* genes was then determined using RT-PCR, and the message levels were compared against those found in respective intact vessels. Briefly, total RNA was extracted from tissues by using the Arcturus PicoPure RNA Isolation Kit (Thermo Fisher Scientific, Waltham, MA, USA) with on-column DNase I treatment (Qiagen, Valencia, CA, USA) according to the manufacturer's protocol. Due to the low volume of tissue in a single EC tube, RNA was eluted with 24 μl of nuclease-free water. Purified RNA (8 μl) was then used for cDNA synthesis via reverse transcription using random hexamer and oligo (dT) primers, and SuperScript III First-Strand Synthesis System (Thermo Fisher Scientific). PCR was performed in a reaction mixture containing first-strand cDNA as the template (2 μl), 2 mM $MgCl_2$, 0.25 μM primers, 0.2 mM deoxynucleotide triphosphates and GoTaq Flexi DNA polymerase (Promega, Madison, WI, USA). The PCR programme comprised an initial denaturation step at 95°C for 4 min, followed by 35 cycles of denaturation for 30 s at 95°C, annealing 30 s at 56°C and elongation for 30 s at 72°C, and a final extension step at 72°C for 5 min. PCR amplification products were separated on a 2% agarose gel by electrophoresis, stained with SYBR-Safe (Thermo Fisher Scientific) and visualized by UV transillumination. Forward and reverse primers used for this study and the expected size of amplicons are listed in Table 1.

Mathematical model: Ca^{2+} and electrical signalling of lymphatic endothelium

The mathematical model of LECT Ca^{2+} signalling and electrophysiology was adapted from a model developed for mesenteric vascular endothelial cells (Silva *et al.* 2007). The plasma membrane is modelled based on the Hodgkin–Huxley model, which has been used for a variety of cell types (e.g. neurons and cardiomyocytes) (Lindblad *et al.* 1996; Yang *et al.* 2003; Koenigsberger *et al.* 2005; Silva *et al.* 2007). In addition to Ca^{2+}, the dynamics of all major ions (Na^+, K^+ and Cl^-) are included (see Fig. 7) to provide a comprehensive analysis of ion fluxes via ion channels, transporters, pumps and exchangers

that underlie regulation of V_m at rest and during the time course of a stimulus (e.g. ACh). A detailed discussion of how the mathematical modelling was performed now follows, with a list of the parameters used in Table 2.

The LECT plasma membrane is assumed to act as a capacitor, and the ion channels and pumps are regarded as parallel paths (Diep *et al.* 2005). The membrane potential (V_m) is calculated using Kirchhoff's law by:

$$\frac{dV_m}{dt} = -\frac{1}{C_m}(I_{TRP} + I_{TRPV4} + I_{Orai} + I_{VRAC} + I_{CaCC}$$
$$+ I_{Kir} + I_{Kleak} + I_{NaK} + I_{PMCA}) \quad (1)$$

where C_m is membrane capacitance and the currents in the parentheses are trans-plasmalemmal ionic currents. The Nernst Potential (E) of each individual ion was calculated using:

$$E_Y = \frac{RT}{z_Y F} \ln\left(\frac{[Y]_o}{[Y]_i}\right) \quad (2)$$

where Y indicates K^+, Na^+, Ca^{2+} or Cl^- and z_Y is $+1$, $+1$, $+2$ and -1 for K^+, Na^+, Ca^{2+} and Cl^-, respectively. $[Y]_i$ indicates intracellular and $[Y]_o$ extra-cellular concentrations. A lumped approach was used to model the reactions and transports inside the LECT. The intracellular space was divided into two compartments: the cytosol and the endoplasmic reticulum (ER). Each ion or protein was assumed to be homogenously distributed in the cytosolic space, ER compartment, or both. K^+, Na^+ and Cl^- can all diffuse through the intracellular space while the ER membrane is assumed to be impermeable to Ca^{2+}, IP_3, calmodulin and other proteins such that their flux is defined through membrane channels and transporters while IP_3–IP_3 receptor (IP_3R) interactions were assumed to be the main pathway for Ca^{2+} release from the ER. Although ryanodine–ryanodine receptor inter-actions have been shown to release Ca^{2+} from ER stores, particularly in excitable cells (Fill & Copello, 2002), they were excluded from the present model because of the lack of supporting data from lymphatic endothelium. Thus, the ER stores denote IP_3-sensitive Ca^{2+} stores, which were modelled using the same equations as Silva and colleagues (2007).

IP_3R current:

$$I_{IP_3R} = \bar{I}_{IP_3R} \frac{[IP_3]^{3.8}}{[IP_3]^{3.8} + K_{m,IP_3}^{3.8}} P_{i,IP_3R} \left([Ca^{2+}]_{IS}\right.$$
$$\left. - [Ca^{2+}]_i\right) \quad (3)$$

$$P_{i,IP_3R} = \frac{K_{i,Ca_i}^{3.8}}{[Ca^{2+}]_i^{3.8} + K_{i,Ca_i}^{3.8}} \quad (4)$$

Sarco(endo)plasmic reticulum Ca^{2+}-ATPase (SERCA) current:

$$I_{SERCA,IS} = \bar{I}_{SERCA,IS} \left(\frac{[Ca^{2+}]_i}{[Ca^{2+}]_i + K_{SERCA,IS}}\right)^2 \quad (5)$$

ER leak current:

$$I_{leak,IS} = k_{leak,IS} \left([Ca^{2+}]_{IS} - [Ca^{2+}]_i\right)^2 \quad (6)$$

Mathematical model: transmembrane currents of lymphatic endothelium

Ions can pass through the plasma membrane either through specific channels or via pumps driven by consumption of ATP. Among the ion pumps, we included, Na^+–K^+-ATPase (I_{NaK}) and Ca^{2+}-ATPase (I_{PMCA}), and removed the Na^+/Ca^{2+} exchanger (I_{NCX}) and the Na^+–K^+–Cl^- cotransporter (I_{NKCC}) due to lack of evidence for their presence in the LECTs.

Na^+–K^+-ATPase current:

$$I_{NaK} = \bar{I}_{NaK} \frac{[K^+]_o}{[K^+]_o + K_{NaK,K_o}} \frac{[Na^+]_i^{1.5}}{[Na^+]_i^{1.5} + K_{NaK,Na_i}^{1.5}}$$
$$\times \frac{V_m + 135.1}{V_m + 300} \quad (7)$$

Ca^{2+}-ATPase current:

$$I_{PMCA} = \bar{I}_{PMCA} \frac{[Ca^{2+}]_i^{n_{PMCA}}}{[Ca^{2+}]_i^{n_{PMCA}} + K_{PMCA,Ca_i}^{n_{PMCA}}} \quad (8)$$

The most important difference between blood ECs and lymphatic ECs is our evidence for the lack of Ca^{2+}-activated K^+ channel currents (I_{SK} and I_{IK}) in LECTs, which led to removal of I_{SK} and I_{IK} from the model. Additionally, we have replaced the non-selective cation channel (I_{NSC}) and store-operated cation channel (I_{SOC}) in the model of Silva and colleagues (2007) with the Ca^{2+} release-activated Ca^{2+} channel (I_{Orai}; Ruhle & Trebak, 2013), the transient receptor potential vanilloid 4 channel (I_{TRPV4}), a composite term for the remaining transient receptor potential channels (I_{TRP}; Hill-Eubanks *et al.* 2014) and the K^+ leak channel (I_{Kleak}). In part, these modifications were made to implement recent data on the molecular mechanisms underlying store-operated and non-selective cation currents. Herein, we explain those currents that are new while adapting equations developed previously (Silva *et al.* 2007; Hald *et al.* 2015).

Results from electrophysiological experiments in the current study suggest that in addition to the sustained increase in $[Ca^{2+}]_i$, the LECT membrane most likely depolarizes due to a subset of TRP channels (including TRPV4) being activated through ACh or a downstream

Table 2. Model parameters for lymphatic endothelium

Parameter	Description	Initial estimate	Model value*	Reference
C_m	Plasma membrane capacitance	14 pF		Silva et al. (2007)
A_m	Plasma membrane surface area	584 μm^2		Voets et al. (1999)
k_B	Boltzmann constant	1.38×10^{-23} m^2 kg s^{-2} K^{-1}		—
vol_i	Intracellular volume	1.173 pl		Silva et al. (2007)
vol_{Ca}	Cytosolic volume available to Ca^{2+}	0.912 pl		Silva et al. (2007)
vol_{IS}	Endoplasmic reticulum volume	0.335 pl		Silva et al. (2007)
R	Gas constant	8.314 J mol K^{-1}		—
T	Temperature	303 K		Experiments
F	Faraday constant	96485.33 C mol^{-1}		—
$[K^+]_o$	Extracellular K^+ concentration	4.7 mM		Experiments
$[Na^+]_o$	Extracellular Na^+ concentration	151.1 mM		Experiments
$[Ca^{2+}]_o$	Extracellular Ca^{2+} concentration	2 mM		Experiments
$[Cl^-]_o$	Extracellular Cl^- concentration	155.6 mM		Experiments
$\bar{I}_{IP_3R}$	Maximum IP_3R current	4.67×10^6 pA mm^{-1}	3.16×10^6 pA mm^{-1}	Silva et al. (2007)
K_{m,IP_3}	$[IP_3]$ for half-maximal IP_3R current	1.6 μM		Silva et al. (2007)
$K_{i,Cai}$	$[Ca^{2+}]_i$ for half-maximal Ca^{2+}-dependent inhibition of IP_3R current	1.0 μM		Silva et al. (2007)
$\bar{I}_{SERCA,IS}$	Maximum SERCA current	0.88 pA		Silva et al. (2007)
$K_{SERCA,IS}$	$[Ca^{2+}]_i$ for quarter-maximal SERCA current	0.15 μM		Silva et al. (2007)
$k_{leak,IS}$	ER leak constant for Ca^{2+}	0.0176 pA mm^{-2}	3.52 pA mm^{-2}	Silva et al. (2007)
$\bar{I}_{NaK}$	Maximum NaK current	22.6 pA		Silva et al. (2007)
$K_{NaK,Ko}$	$[K^+]_o$ for half-maximal NaK activation	1.32 mM		Silva et al. (2007)
$K_{NaK,Nai}$	$[Na^+]_i$ for half-maximal NaK activation	14.5 mM		Silva et al. (2007)
$\bar{I}_{PMCA}$	Maximum PMCA current	2.67 pA	4.30 pA	Silva et al. (2007)
$K_{PMCA,Cai}$	$[Ca^{2+}]_i$ for half-maximal PMCA activation	260 nM		Silva et al. (2007)
n_{PMCA}	Hill coefficient for $[Ca^{2+}]_i$ dependency of PMCA current	1.4, 1.7, 4.4	3.0	Silva et al. (2007), Wiesner et al. (1996)
$P_{TRPV4,Na,max}$	Maximum permeability of TRPV4 to Na^+	3.95×10^{-7} cm s^{-1}	2.08×10^{-7} cm s^{-1}	Silva et al. (2007)
$P_{ratio,TRPV4}$	Permeability ratio of Ca^{2+} to Na^+ for TRPV4 (P_{Ca}/P_{Na})	6		Gees et al. (2010)
K_{TRPV4}	ER depletion for half-maximal TRPV4 activation	0.25 mM		Experiments
n_{TRPV4}	Hill coefficient for $[Ca^{2+}]_{IS}$ dependency of TRPV4 current	3		Experiments
$P_{Orai,max}$	Maximum permeability of Orai to Ca^{2+}	1.15×10^{-7} cm s^{-1}	1.25×10^{-6} cm s^{-1}	Silva et al. (2007)
K_{Orai}	ER depletion for half-maximal Orai activation	0.25 mM		Experiments
n_{Orai}	Hill coefficient for $[Ca^{2+}]_{IS}$ dependency of Orai current	3		Experiments
P_{TRP}	Permeability of TRP to Na^+ and Ca^{2+}	$(1.3–5.3) \times 10^{-8}$ cm s^{-1}	2.01×10^{-8} cm s^{-1}	Experiments
P_{Kleak}	Permeability of leak channels to K^+	1.3×10^{-7} cm s^{-1}	1.26×10^{-7} cm $^{-1}$	Experiments
G_{Kir}	Kir conductance constant	0.142 nS $mM^{-0.5}$	0.051 nS $mM^{-0.5}$	Silva et al. (2007)
n_{Kir}	Kir power constant	0.5		Silva et al. (2007)
$\Delta V_{Kir,h}$	K^+ driving force at half Kir channel conductance	39.4 mV		Silva et al. (2007)

(Continued)

Table 2. Continued

Parameter	Description	Initial estimate	Model value*	Reference
ν_{Kir}	Slope factor of Kir conductance	7.08 mV		Silva et al. (2007)
G_{VRAC}	VRAC conductance	0.381 nS	0.0381 nS	Silva et al. (2007)
G_{CaCC}	Maximum CaCC conductance	37.4 nS	3.74 nS	Silva et al. (2007)
K_{CaCC}	$[Ca^{2+}]_i$ at which CaCC Ca^{2+}-dependent open probability is 50%	287 nM		Silva et al. (2007)
n_{CaCC}	Hill coefficient of CaCC Ca^{2+}-dependent open probability function	1.89		Silva et al. (2007)
$V_{CaCC,h}$	Membrane potential for half CaCC conductance	662 mV		Silva et al. (2007)
ν_{CaCC}	Slope factor of CaCC conductance	132 mV		Silva et al. (2007)
$k_{B,on}$	Forward binding rate for Ca^{2+}–calmodulin binding	100 $mM^{-1} \cdot ms^{-1}$		Silva et al. (2007)
$k_{B,off}$	Backward binding rate for Ca^{2+}–calmodulin binding	0.3 ms^{-1}		Silva et al. (2007)
B_T	Total concentration of Ca^{2+} binding sites in the cytosol	0.12 mM		Silva et al. (2007)
CSQN	Total concentration of Ca^{2+} binding sites in the ER stores	8.8 mM		Prins & Michalak (2011)
K_{CSQN}	Dissociation constant for CSQN	2 mM		Prins & Michalak (2011)
k_{DIP_3}	Degradation rate for IP$_3$	2×10^{-3} ms^{-1}		Silva et al. (2007)
$Q_{GIP_3,SS}$	Agonist-mediated steady state IP$_3$ generation rate	5.5×10^{-8} mM ms^{-1}		Silva et al. (2007)
τ_{IP_3}	Time constant for IP$_3$ generation rate change	33 s		Silva et al. (2007)

*If the parameter value used in the model is different from the initial estimates from references. CSQN, calsequestrin.

signalling event. The secondary sustained increase in Ca^{2+} can be explained by stromal interaction molecule 1 (STIM1)-mediated Orai current. Importantly, two recent studies provide strong evidence for the expression of Orai1 in murine lymphatic endothelium (Choi *et al.* 2017*a*,*b*). However, the level of depolarization we have observed requires involvement of TRP channels. The V_m of LECs (~-70 mV) is closer to the equilibrium potential of K^+ than that of Cl^- channels. $P_{TRPV4,Na,max}$ was chosen to fit the depolarization of V_m relative to our experimental data. Based on the evidence on cooperation of TRP channels in store-operated current, Orai channel permeability ($P_{Orai,max}$) was selected to have similar currents to TRPV4 during ER depletion (Liao *et al.* 2008; Ma *et al.* 2011). TRP channels have a wide range of P_{Ca}/P_{Na} from <1 to >100 (Clapham *et al.* 2005; Gees *et al.* 2010). We have assumed P_{Ca}/P_{Na} of 1 for the basal TRP channels and P_{Ca}/P_{Na} of 6 for TRPV4 ($P_{ratio,TRPV4}$) (Gees *et al.* 2010). The Hill coefficient and half-maximal activation concentration of ER depletion for both TRPV4 and Orai was selected to capture the dynamics of the second phase of Ca^{2+} entry. Adjustment of the K^+ leak channel permeability (P_{Kleak}) ensured that our model matches the consistent observation of ~11 mV depolarization after I_{Kir} blockade by $BaCl_2$ (see Fig. 10*H*). Finally, the effect of GSK101 for TRPV4 activation was modelled by gradually opening the TRPV4 channels until they reached maximum permeability.

Data analysis

Analyses included: (1) fluorescence emission collected at 510 nm and expressed as the ratio during excitation at 340 and 380 nm (F_{340}/F_{380}); (2) change in F_{340}/F_{380} ratio ($\Delta F_{340}/F_{380}$) = peak response F_{340}/F_{380} − preceding baseline F_{340}/F_{380}; (3) resting V_m (mV); (4) change in V_m (ΔV_m) = peak response V_m − preceding baseline V_m. All summary data reflect values averaged over 10 s during stable recordings. Statistical analyses (GraphPad Prism 5; GraphPad Software, Inc., La Jolla, CA, USA) included Student's paired and unpaired *t* test. Differences were accepted as statistically significant with $P < 0.05$. Summary data are presented as means ± SEM unless specified otherwise. One EC tube (either arteriolar or lymphatic) or intact lymphatic vessel was studied from each mouse for a given experimental protocol with '*n*' reflecting the number of independent EC tubes or lymphatic vessels.

Results

The present experiments were designed to determine whether the requisite machinery of the EDH pathway (e.g. SK_{Ca}/IK_{Ca} activation) was present for transducing $[Ca^{2+}]_i$ increases into hyperpolarization in native intact

lymphatic endothelium. Initial experiments addressed whether pharmacological agonists and antagonists of SK_{Ca}/IK_{Ca} as well as other K^+ channels associated with blood vessel endothelium (e.g. inward-rectifying K^+ (K_{IR}) channels, ATP-sensitive K^+ (K_{ATP}) channels; Jackson, 2005) influenced the resting V_m of lymphatic endothelium. Initial findings prompted ensuing analyses of the dynamics of both $[Ca^{2+}]_i$ and V_m in response to the well-defined M_3 receptor agonist ACh (intracellular ER Ca^{2+} release followed by Ca^{2+} influx; Himmel *et al.* 1993) and the TRPV4 agonist GSK101 (Ca^{2+} influx; Thorneloe *et al.* 2008). These functional data were complemented by computational modelling to resolve the roles of TRP channels and ions (e.g. Na^+, K^+, Cl^-) underlying the dynamics of Ca^{2+} and electrical signalling in lymphatic endothelium.

K_{IR} channels contribute to resting V_m of lymphatic endothelium but K_{Ca} and K_{ATP} channels do not

Application of agents known to activate K_{Ca} channels and thereby evoke robust hyperpolarization in arterial endothelium caused a pronounced depolarization in lymphatic endothelium. As summarized in Fig. 1*A*, ACh (1 μM) depolarized lymphatic ECs from a resting V_m of -60 ± 7 mV to -33 ± 4 mV ($P < 0.05$), while the TRPV4 agonist GSK101 (100 nM) depolarized lymphatic ECs from -59 ± 3 to -13 ± 3 mV ($P < 0.05$). The K_{IR} channel blocker $BaCl_2$ (100 μM) depolarized V_m from -60 ± 5 to -49 ± 5 mV ($P < 0.05$). In contrast, neither the SK_{Ca}/IK_{Ca} opener NS309 (1 μM) nor inhibition with the combination of apamin (300 nM) + charybdotoxin (100 nM) altered resting V_m significantly (ΔV_m, 1–3 mV). The large-conductance K_{Ca} channel (BK_{Ca}) blocker paxilline (1 μM), the K_{ATP} channel opener levcromakalim (10 μM) and the K_{ATP} channel inhibitor glyburide (10 μM) were also without significant effect on resting V_m (ΔV_m, 1–2 mV). Collectively, these findings suggested that K_{Ca} channels were not expressed by lymphatic endothelium. We therefore performed endpoint RT-PCR to determine whether the genes encoding SK_{Ca}/IK_{Ca} channels (i.e. *Kcnn3* and *Kcnn4*, respectively) were transcribed. As shown in Fig. 1*B*, whole popliteal arteries and whole lymphatic vessels expressed mRNA for *Kcnn3* and *Kcnn4*. In contrast, the isolated lymphatic endothelium was devoid of detectable message for *Kcnn3* or *Kcnn4*, while the isolated arterial endothelium showed abundant expression for both of these genes.

Lack of EDH in lymphatic endothelium: depolarization occurs with increased $[Ca^{2+}]_i$ in response to ACh

We next evaluated $[Ca^{2+}]_i$ dynamics simultaneously with V_m responses induced by ACh in LECTs while confirming EDH signalling in the endothelium of resistance arteries

isolated from the same anatomical site (Fig. 2*A* and *B*). Figure 2*C* illustrates a classic arterial endothelial response of $[Ca^{2+}]_i$ dynamics to ACh, whereby an initial rapid rise in F_{340}/F_{380} (due to intracellular release from the ER) is followed by a 'plateau' phase attributable to Ca^{2+} influx through the plasma membrane (Cohen & Jackson, 2005; Socha *et al.* 2012; Behringer & Segal, 2015). Furthermore, arterial endothelium rapidly hyperpolarized from -31 ± 5 to -69 ± 4 mV during peak $[Ca^{2+}]_i$ (Fig. 2*E* and *H*, $n = 4$), with changes in V_m mirroring those of $[Ca^{2+}]_i$ in both magnitude and time course (Fig. 2*C* and *E*). In contrast, whereas the dynamics of $[Ca^{2+}]_i$ responses to ACh in LECTs were similar to that in AECTs (Fig. 2*D* and *G*), V_m in LECTs underwent a gradual depolarization from -66 ± 3 to -45 ± 3 mV in response to ACh exposure (Fig. 2*F* and *H*). Thus, during exposure to ACh, hyperpolarization occurs simultaneously with an increase in $[Ca^{2+}]_i$ in arterial endothelium, whereas a slow depolarization occurs in lymphatic endothelium.

To address whether depolarization in response to ACh occurred in LECs of intact vessels, the endothelial V_m in isolated and pressurized Ing-Ax lymphatic vessels was measured. From a resting V_m of -64 ± 3 mV ($n = 3$), LECs depolarized by 51 ± 2 mV to -13 ± 2 mV in response to ACh (1 μM; Fig. 3*A* and *B*). These data illustrate

that LEC V_m depolarization to ACh occurs irrespective of surrounding smooth muscle cells that exhibit spontaneous action potentials (Von der Weid *et al.* 2014).

Depolarization of lymphatic endothelium during ACh stimulation requires Ca^{2+} influx

As observed for arterial endothelium, removal of 2 mM $[Ca^{2+}]_o$ (Cohen & Jackson, 2005; Socha *et al.* 2011; Behringer & Segal, 2015) or treatment with the non-selective cation channel blocker $LaCl_3$ (Cohen & Jackson, 2005) eliminated the plateau phase of the $[Ca^{2+}]_i$ response in lymphatic endothelium during exposure to ACh, while the initial peak $[Ca^{2+}]_i$ response was preserved (Fig. 4*A*, *B*, *E* (left panel) and *F* (left panel); compare to Fig. 2*D* and *G*). In reference to Figure 2*D* and *F*, depolarization to ACh still occurred along with the peak phase of the $[Ca^{2+}]_i$ response and persisted despite the absence of the plateau phase; however, removal of extracellular Ca^{2+} reduced depolarization by $\sim$50% (Fig. 4*C* and *E* (right panel)). When cation influx was blocked with $LaCl_3$, depolarization was eliminated (Fig. 4*D* and *F* (right panel)). These findings suggest that progressive depolarization to ACh in LECs depends upon a sustained increase in $[Ca^{2+}]_i$. The residual depolarization
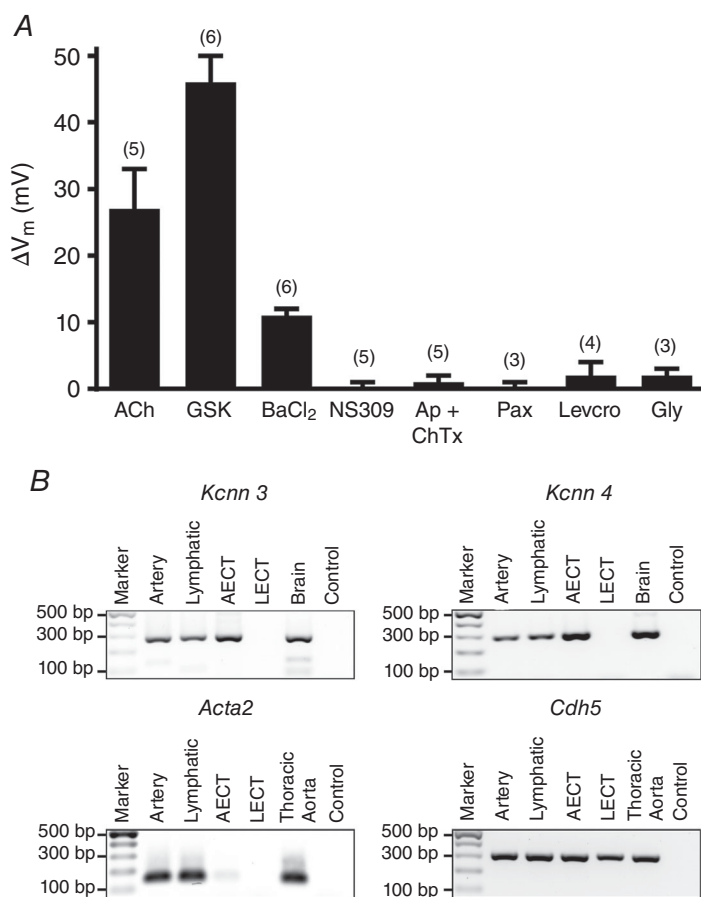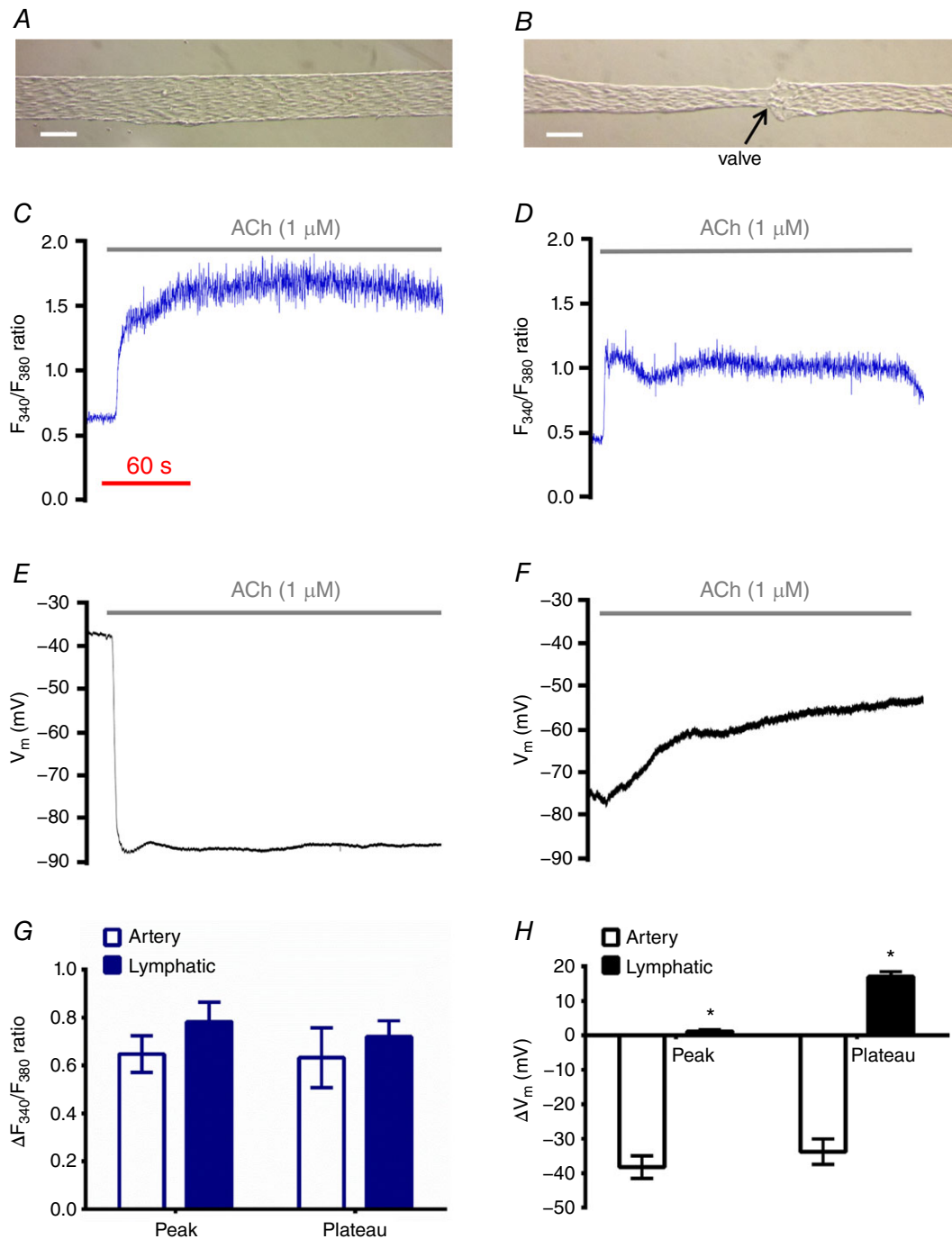
Figure 1. Lack of K_{Ca} channel activity governing V_m in lymphatic endothelium and absence of SK_{Ca} and IK_{Ca} transcript expression

A, respective bars indicate changes in resting V_m in response to acetylcholine (ACh; 1 μM), TRPV4 activation (GSK101; 100 nM), inward rectifying K^+ channel blockade ($BaCl_2$; 100 μM), SK_{Ca}/IK_{Ca} activation (NS309; 1 μM), SK_{Ca}/IK_{Ca} blockade (apamin (Ap; 300 nM) + charybdotoxin (ChTx; 100 nM)), large conductance Ca^{2+}-activated K^+ (BK_{Ca}) channel block (paxilline (Pax); 1 μM), ATP-sensitive K^+ (K_{ATP}) channel activation (levcromakalim (Levcro); 10 μM) and K_{ATP} channel blockade (glyburide (Gly); 10 μM)). Depolarization ($P < 0.05$) occurred in response to ACh, GSK and $BaCl_2$ for '(n)' experiments. Resting V_m of LECTs varied from ~ -50 to -80 mV, and therefore respective treatment effects are reported as changes (ΔV_m) from resting V_m preceding treatment. *B*, endpoint PCR images indicating mRNA expression of SK_{Ca} (*Kcnn3*), IK_{Ca} (*Kcnn4*), smooth muscle α-actin (*Acta2*) and vascular endothelial cadherin (*Cdh5*) for individual popliteal artery, collecting lymphatic vessel, arterial endothelial cell tube (AECT) and lymphatic endothelial cell tube (LECT). The intact artery and intact lymphatic vessel both expressed mRNA for SK_{Ca} and IK_{Ca}. In contrast, the LECT did not express mRNA for either SK_{Ca} or IK_{Ca}, while the AECT expressed abundant mRNA for both of these genes. Brain and thoracic aorta were used as positive controls for K_{Ca} channels and cell type-specific markers (i.e. smooth muscle α-actin and endothelial cadherin), respectively. For negative controls (Control), no template was loaded.

Figure 2. Lack of EDH in lymphatic endothelium

A, brightfield image of an AECT isolated from a popliteal artery. *B*, as in *A* for a LECT isolated from a popliteal lymphatic vessel; note the valve (arrow) in *B* that is absent in *A*. Scale bars (white) in *A* and *B* indicate 50 μm. *C*, recording of Fura-2 fluorescence response to ACh for an AECT. *D*, as in *C* for a LECT. In both traces, note rapid increase in the F_{340}/F_{380} ratio ('peak'; $\leq$20 s of ACh onset) that was sustained (i.e. 'plateaued') for the duration of ACh exposure. *E*, simultaneous recording of V_m during ACh from an AECT. *F*, as in *E* from a LECT. Note that the change V_m in *E* is hyperpolarization that mirrors dynamics in $[Ca^{2+}]_i$ in *C*. In contrast a gradual depolarization occurs in in *F* that begins approximately during the $[Ca^{2+}]_i$ peak phase in *D*. *G*, summary of changes in F_{340}/F_{380} values for AECTs and LECTs in response to ACh during the peak ($\leq$20 s of ACh onset) and plateau (90 s following peak) phase of responses. *H*, as in *G* for corresponding changes in V_m. Data represent $n = 4$ AECTs and $n = 13$ LECTs. *$P < 0.05$, responses different from artery.

during the absence of $[Ca^{2+}]_o$ may be due to Na^+ influx that can be abolished by blocking TRP channels permeable to both Ca^{2+} and Na^+ (e.g. TRPV4) by $LaCl_3$. This hypothesis was tested using the TRPV4 opener GSK101 in LECTs from wild-type (WT) mice and with LECTs isolated from $Trpv4^{-/-}$ mice.

Depolarization of lymphatic endothelium occurs via TRPV4 channels

TRPV4 channels are integral to agonist-mediated Ca^{2+} influx across plasma membranes of arterial endothelium (Zhang *et al.* 2009; Sonkusare *et al.* 2012; Qian *et al.* 2014). However, these channels are also permeable to Na^+ and are only moderately more selective for Ca^{2+} over Na^+ ($P_{Ca}/P_{Na} \approx 6$) compared to other Ca^{2+}-permeable cation channels such as TRPV5 and TRPV6 ($P_{Ca}/P_{Na} > 100$) (Clapham *et al.* 2005). Membrane permeability to Na^+ is functionally important given its integral role during excitation and depolarization of mammalian cells (Hille, 2001). In response to opening TRPV4 channels with GSK101, wild-type LECTs responded with a robust increase in $[Ca^{2+}]_i$ (Fig. 5A and G) coincident with depolarization (Fig. 5D and H). A key finding from these experiments is

Figure 3. Acetylcholine depolarizes endothelium of intact lymphatic vessels
A, recording of V_m in the endothelial layer of a pressurized (3 cmH_2O) Ing-Ax lymphatic collecting vessel at rest and during ACh (1 μM). Note ~50 mV depolarization to ACh treatment. *B*, summary of lymphatic endothelium resting V_m in pressurized Ing-Ax vessels and in response to ACh. *$P < 0.05$, response different from control. Data represent $n = 3$ Ing-Ax lymphatic vessels, each from a separate C57BL/6 mouse.

that depolarization to GSK101 was sustained (Fig. 5E) in the absence of extracellular Ca^{2+} or of a rise in $[Ca^{2+}]_i$ (Fig. 5B) but was eliminated in the presence of $LaCl_3$ (Fig. 5F).

In LECTs isolated from $Trpv4^{-/-}$ mice, both the rise in $[Ca^{2+}]_i$ and the depolarization to ACh ($\Delta F_{340}/F_{380}$: 0.35 ± 0.12, ΔV_m: 6 ± 2 mV, $n = 4$) were attenuated significantly ($P < 0.05$) compared to wild-type C57BL/6 mice ($\Delta F_{340}/F_{380}$: 0.72 ± 0.07, ΔV_m: 17 ± 2 mV, $n = 13$) (Fig. 6A, C and E *vs.* Fig. 2D, F, G and H). Further, $[Ca^{2+}]_i$ and depolarization responses to GSK were absent in LECTs from $Trpv4^{-/-}$ mice (Fig. 6B, D and F; $\Delta F_{340}/F_{380}$: -0.01 ± 0.02, ΔV_m: -2 ± 3 mV; $n = 5$ LECTs isolated from 4 mice).

These findings collectively illustrate that TRPV4 channels play an integral role in lymphatic endothelium signalling, with both Ca^{2+} and Na^+ influx contributing to membrane depolarization in response to ACh. We used computational modelling to resolve the contributions of Ca^{2+} and Na^+ with respect to other ions (e.g. K^+, Cl^-) and membrane channels (e.g. Orai, volume-regulated anion Cl^- channels) in lymphatic endothelium.

Mathematical modelling: ionic fluxes and electrical dynamics in lymphatic endothelium

Computational modelling for ion channels in LECs was adapted from models published for ion channels in blood vessel endothelial cells (Fig. 7) (Wiesner *et al.* 1996; Silva *et al.* 2007; Gees *et al.* 2010; Prins & Michalak, 2011).

ACh treatment. Figure 8A illustrates a two-phase response (i.e. 'peak' and 'plateau') similar to what we resolved experimentally for lymphatic endothelium (Fig. 2D), whereby depolarization occurs in parallel (compare Figs 2F and 8D). When extracellular Ca^{2+} is removed, the plateau is abolished (compare Figs 4A and 8B) but there is a discrepancy in how depolarization is affected (compare Figs 4C and 8E), attributable to the manner by which TRPV4 and Orai activation is modelled. When $[Ca^{2+}]_o$ falls, ER calcium is released leading to opening of TRPV4 and the storage-operated Ca^{2+} channel, Orai (Ruhle & Trebak, 2013). TRPV4 channels then allow sodium entry, resulting in the depolarization in the model (Fig. 8E). Computational blocking of TRPV4 and Orai mimics treatment with the non-selective cation blocker $LaCl_3$, whereby depolarization is effectively abolished (Fig. 8F) in the presence of a significantly reduced $[Ca^{2+}]_i$ plateau during stimulation with ACh (compare Figs 4B and 8C). Similar to data obtained from $Trpv4^{-/-}$ mice (see Fig. 6A, C and E), the model also shows that the absence of TRPV4 alone is sufficient to abolish the depolarization (Fig. 8F) while both TRPV4 and Orai currents need to be eliminated to remove the Ca^{2+} plateau in response to ACh (Fig. 8C).
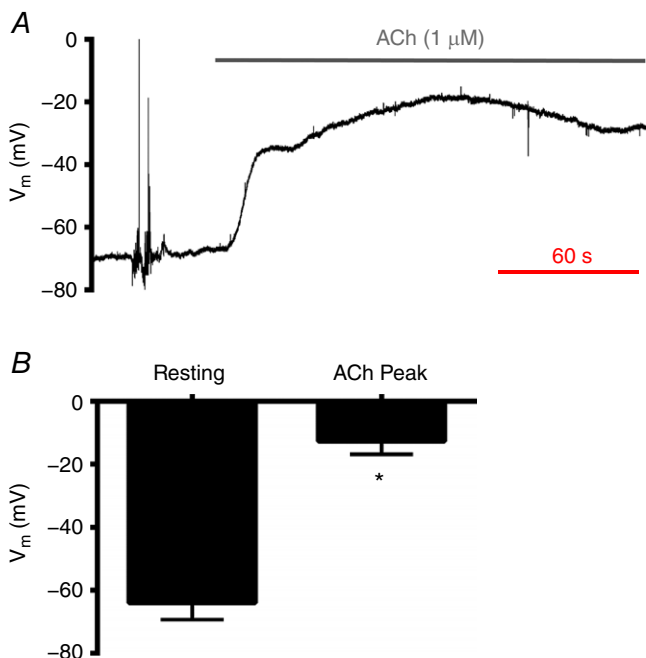
GSK101 treatment. Figure 9 illustrates the model's prediction of a parallel increase in $[Ca^{2+}]_i$ (Fig. 9A) and depolarization (Fig. 9D) in response to TRPV4 activation with GSK101, which emulate Fig. 5A and D respectively. Despite eliminating the rise in $[Ca^{2+}]_i$ during GSK101 treatment when extracellular Ca^{2+} is absent (Figs 5B and 9B), depolarization is not significantly decreased (Figs 5E and 9E). However, elimination of Orai and TRPV4 currents effectively abolish any increase in $[Ca^{2+}]_i$ (Figs 5C and 9C) or depolarization of V_m (Figs 5F and 9F) during
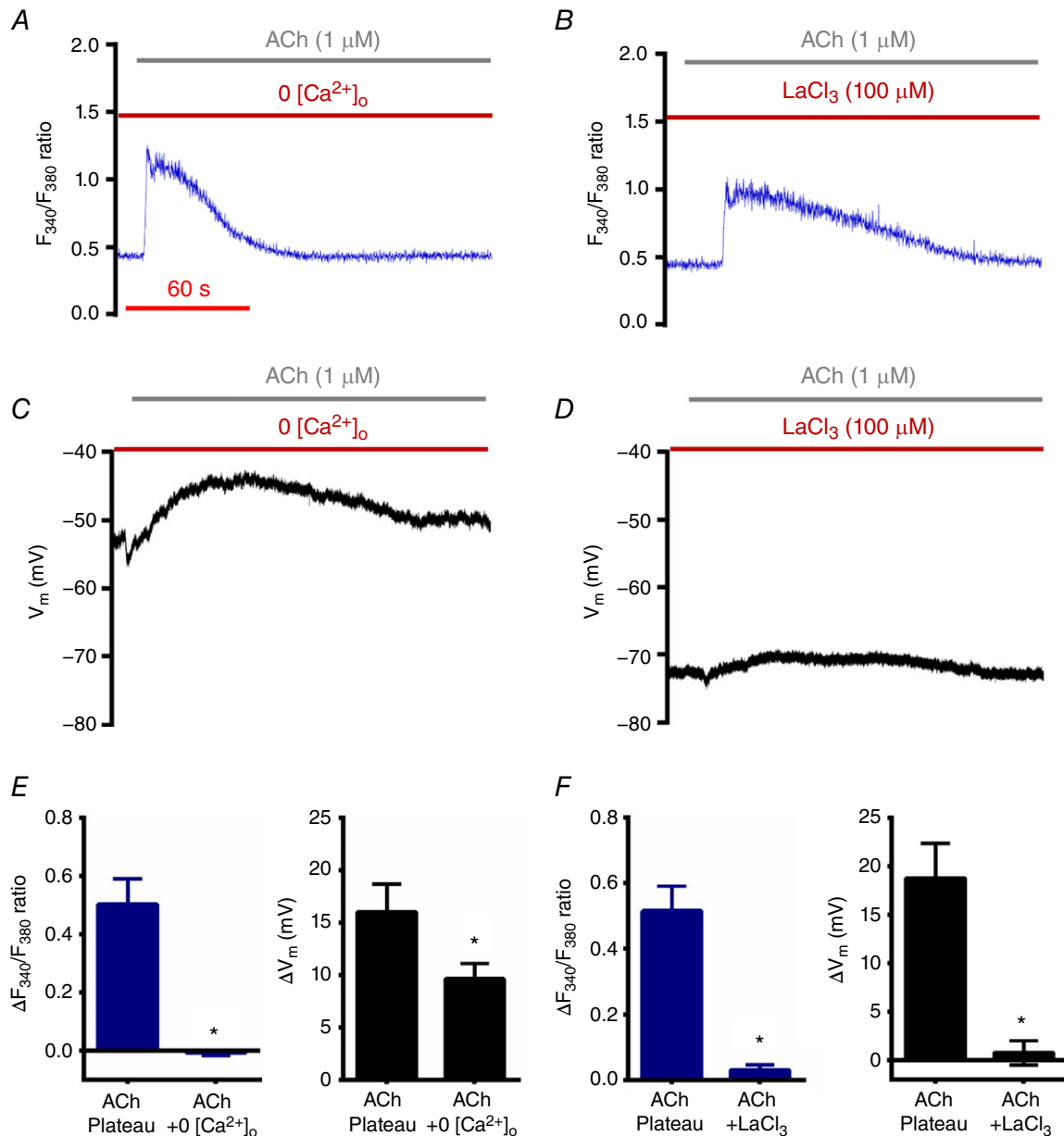
Figure 4. Role of $[Ca^{2+}]_o$ during depolarization of V_m to ACh in lymphatic endothelium
A, recording of Fura-2 fluorescence during ACh in the absence of $[Ca^{2+}]_o$ in a LECT. B, as in A, in the presence of 2 mM $[Ca^{2+}]_o$ and during treatment with LaCl$_3$, a broad-spectrum blocker of Ca^{2+}-permeable channels in the plasma membrane. Note that the plateau phase is abolished in both A and B (compare to Fig. 2D). C, as in A, with recording of V_m. D, as in B, with recording of V_m. Note that depolarization is impaired in C and D (compare to Fig. 2F). E, summary of changes in F_{340}/F_{380} ratio (left) and V_m (right) during the plateau phase (90 s) of the response to ACh in the presence and absence of 2 mM $[Ca^{2+}]_o$. F, as in E, indicating treatment with LaCl$_3$ (+2 mM $[Ca^{2+}]_o$). Values were obtained at the same time points in paired experiments (ACh *versus* ACh + LaCl$_3$) corresponding to the abolished F_{340}/F_{380} plateau ($\Delta F_{340}/F_{380} \approx 0$ recorded, $\sim$ 2.5 min after ACh onset) via treatment with LaCl$_3$. Data represent $n = 5$ paired experiments with ACh $\pm$ 2 mM $[Ca^{2+}]_o$ and $n = 4$ paired experiments with ACh $\pm$ LaCl$_3$. *$P < 0.05$, responses different from ACh (with 2 mM $[Ca^{2+}]_o$) alone.

treatment with GSK101 (note similarity to data obtained from $Trpv4^{-/-}$ mice during GSK101 treatment; Fig. 6B, D and F).

Dynamics in ionic fluxes and open probability of key channels, exchangers and pumps. The strength of the mathematical model is the simultaneous calculation of currents contributed by ion channels, pumps, transporters and exchangers that underlie the depolarization response in lymphatic endothelium, a task that is not feasible using experimental approaches alone within a single study. Figure 10A illustrates the integrated depolarization response at rest ($t < 0$ s) and during ACh stimulation ($t > 0$ s) (compare to Fig. 2F). In response to ACh, the

model predicts that IP_3R is activated, releasing Ca^{2+} from the ER (Fig. 10E), which is then removed from the cytosol by the plasma membrane Ca^{2+}-ATPase (PMCA; Fig. 10F). As the ER Ca^{2+} drops in response to ACh (Fig. 10C), TRPV4 and Orai channels open (Fig. 10F and G) leading to a plateau increase in $[Ca^{2+}]_i$ (Fig. 10D); however, the permeability of TRPV4 to Na^+ leads to depolarization (Fig. 10A). In this model, TRP channels other than TRPV4 appear to play a negligible role in depolarization (Fig. 10F and G). The Na^+–K^+-ATPase (NaK) pump maintains Na^+ and K^+ concentration gradients and currents (Fig. 10G for Na^+ and Fig. 10H for K^+) across the plasma membrane at rest and during ACh (Fig. 10C). Basal Cl^- currents (Fig. 10I) through Ca^{2+}-activated
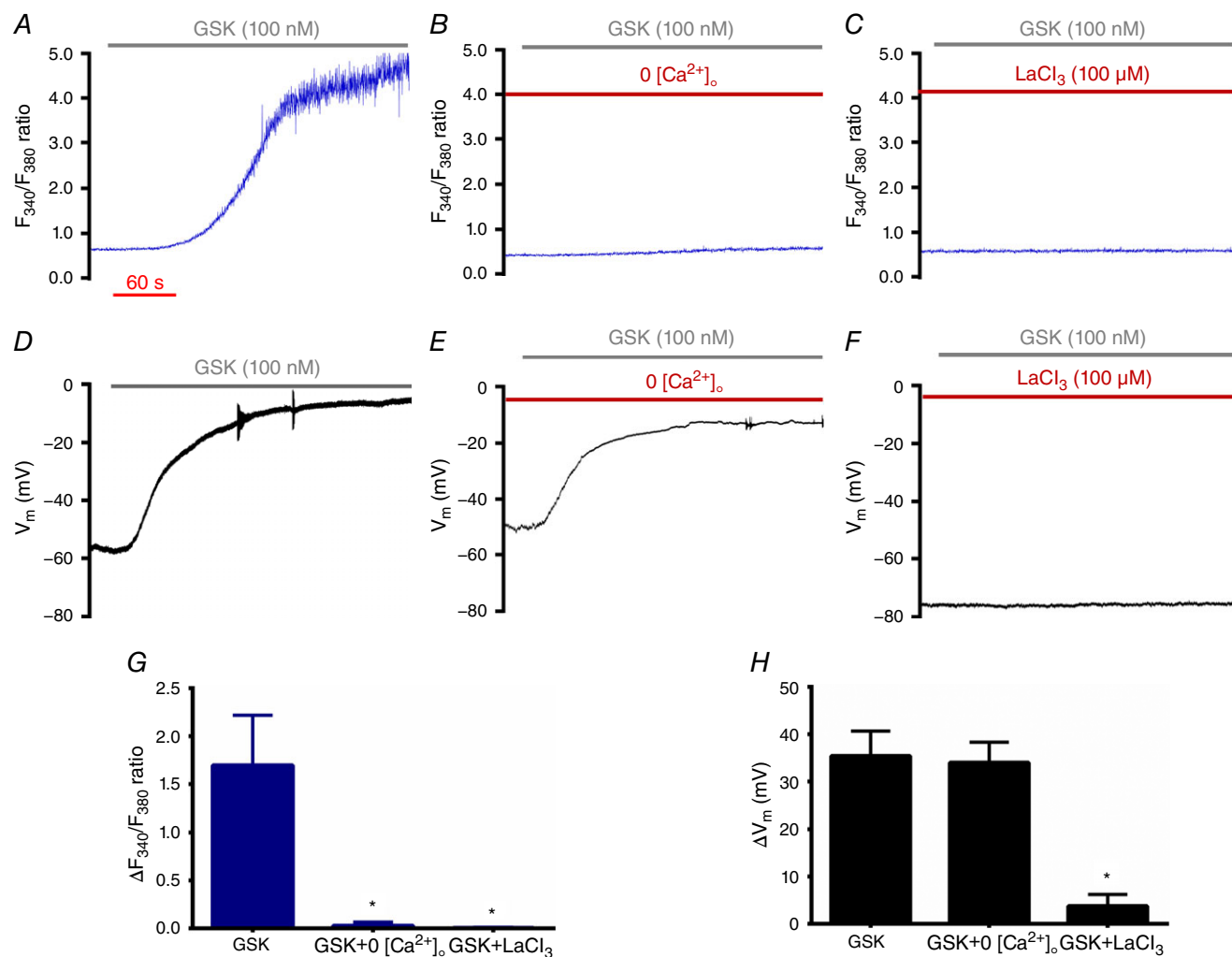

Figure 5. Opening of TRPV4 channels leads to depolarization of lymphatic endothelium
A, recording of Fura-2 fluorescence during GSK101 (with 2 mM $[Ca^{2+}]_o$) in lymphatic endothelium. *B*, as in *A*, with 0 $[Ca^{2+}]_o$. *C*, as in *A*, with LaCl₃. Note that increases in F_{340}/F_{380} are abolished in *B* and *C*. *D*, as in *A*, recording of V_m. *E*, as in *B*, with recording of V_m. *F*, as in *C*, with recording of V_m. Note that the depolarization in *E* (GSK101 + 0 $[Ca^{2+}]_o$) is absent in *F* (GSK101 + LaCl₃). *G*, summary of changes in F_{340}/F_{380} ratio at 3 min following onset of GSK101 with 2 mM $[Ca^{2+}]_o$ present, GSK101 + 0 $[Ca^{2+}]_o$ and with GSK101 + LaCl₃. *H*, as in *G*, for changes in V_m. *P < 0.05, responses different from GSK101 with 2 mM $[Ca^{2+}]_o$. Data represent $n = 5$ experiments for GSK101 with 2 mM $[Ca^{2+}]_o$), $n = 4$ for GSK101 with 0 $[Ca^{2+}]_o$ and $n = 4$ for GSK101 with LaCl₃.

chloride channels (CaCCs) and volume-regulated anion channels (VRACs) are negligible in the absence of Na^+–K^+–Cl^- cotransporters (NKCCs); however, membrane depolarization in response to ACh results in transient Cl^- currents through CaCCs and VRACs.

Altogether, ACh in LECTs triggers internal Ca^{2+} release from the ER which in turn activates non-selective cation channels (or TRPs) in the plasma membrane and, in particular, TRPV4. While Ca^{2+} influx through TRPV4

channels is observed, it is the concomitant influx of Na^+ that primarily underlies the integrated V_m response to ACh in the form of depolarization.

Discussion

The present study has simultaneously monitored membrane potential and intracellular Ca^{2+} in freshly
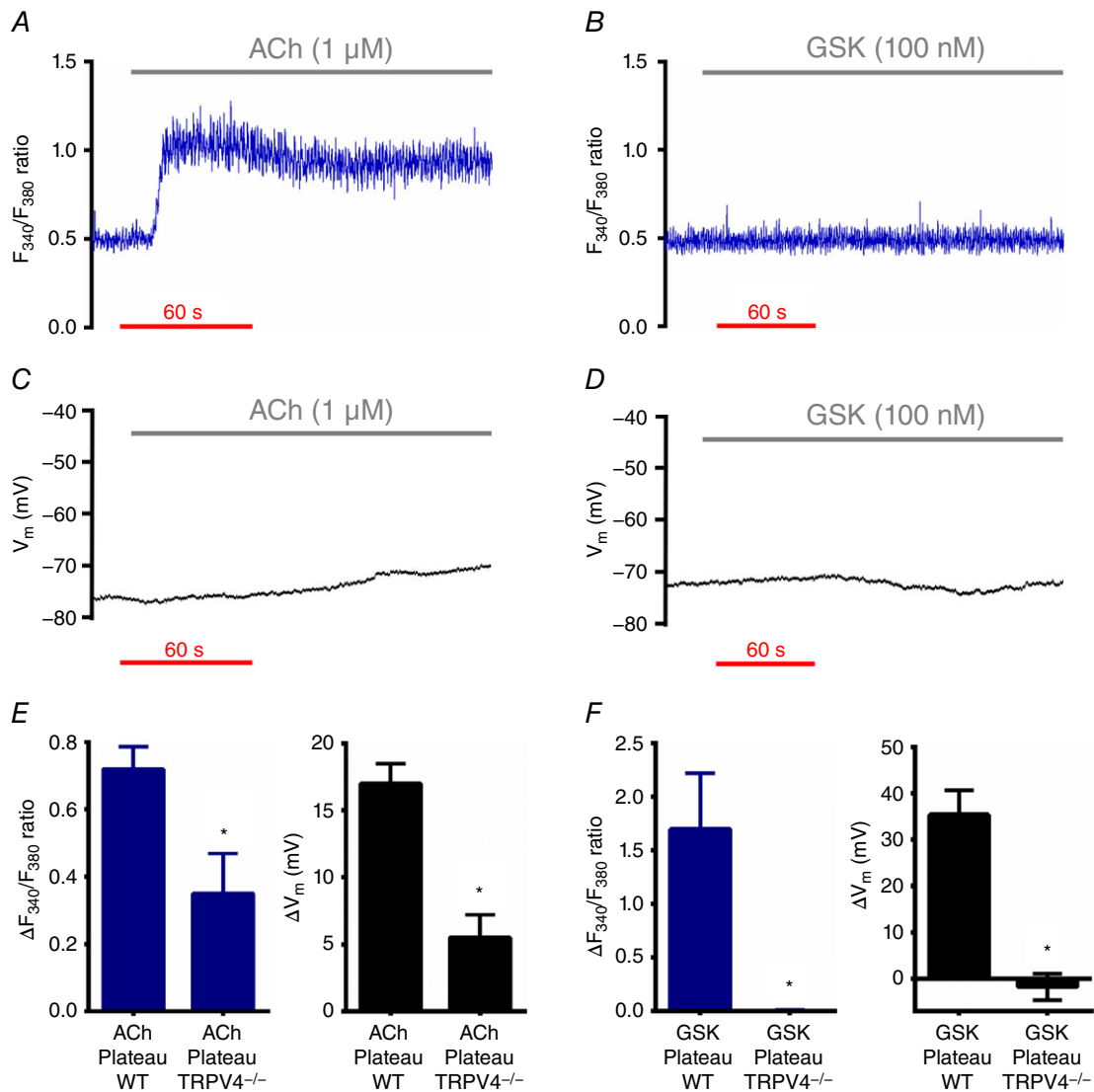
Figure 6. Lack of TRPV4 channels reduces $[Ca^{2+}]_i$ and eliminates depolarization to ACh and GSK101 in lymphatic endothelium
A, recording of Fura-2 fluorescence during ACh with 2 mM $[Ca^{2+}]_o$ in a LECT isolated from a *Trpv4$^{-/-}$* mouse. *B*, as in *A*, with GSK101. *C*, as in a *A*, with recording of V_m. *D*, as in *B*, with recording of V_m. Note that the plateau in F_{340}/F_{380} and depolarization are diminished during ACh treatment (*A* and *C*) and are abolished during GSK101 treatment (*B* and *D*) when compared to LECTs from C57BL/6 (WT) mice. *E*, summary of changes in F_{340}/F_{380} values (left) and V_m (right) during the ACh plateau phase (90 s) in LECTs isolated from WT (*n* = 13) *vs.* *Trpv4$^{-/-}$* mice (*n* = 4). *F*, as in *E*, indicating data at 3 min following onset of GSK101 treatment (WT and *Trpv4$^{-/-}$*; *n* = 5 each). For *E*, WT data during ACh treatment were taken from Fig. 2*G* ($\Delta[Ca^{2+}]_i$) and Fig. 2*H* (ΔV_m). For *F*, WT data during GSK101 treatment were taken from Fig. 5*G* ($\Delta[Ca^{2+}]_i$) and Fig. 5*H* (ΔV_m). **P < 0.05*, responses different between LECTs isolated from WT *versus* *Trpv4$^{-/-}$* mice.

isolated lymphatic endothelial cell tubes for the first time. Complementary experiments and computational modelling have revealed a two-phase response to ACh (i.e. 'peak' and 'plateau') in $[Ca^{2+}]_i$ dynamics that is

mediated through activation of TRPV4 channels and mimics the behaviour reported for endothelium of arterioles and resistance arteries (Cohen & Jackson, 2005; Socha *et al.* 2011; Behringer & Segal, 2015). However,
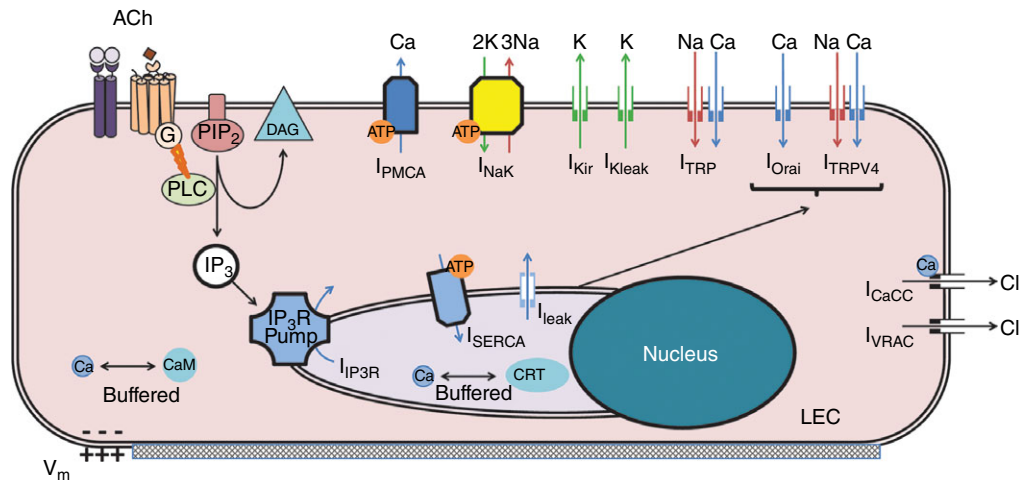

Figure 7. Schematic diagram of ion channels and pumps in computational model of lymphatic endothelium
A variety of channels and pumps are present in LECs; see 'Methods' for detailed description. K^+ currents are in green, Na^+ currents are in red, Cl^- currents are in black and Ca^{2+} currents are in blue. ACh stimulation leads to IP_3 formation and activation of the IP_3R on the endoplasmic reticulum. Calcium ions in the cytosol and endoplasmic reticulum are buffered with calmodulin (CaM) and calreticulin (CRT).
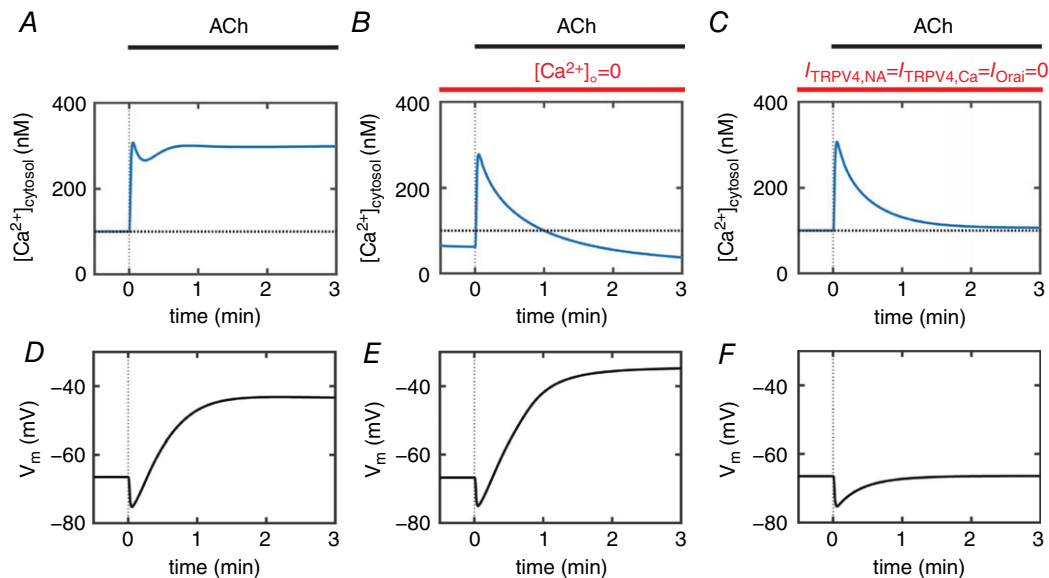
Figure 8. Computational modelling: intracellular Ca^{2+} changes with V_m during stimulation with ACh
A, $[Ca^{2+}]_i$ changes during ACh stimulation in lymphatic endothelium. The pattern of rapid increase in $[Ca^{2+}]_i$ followed by a sustained plateau is similar to the one observed in Fura-2 experiments (Fig. 2*D*). *B*, as in *A*, in the absence of $[Ca^{2+}]_o$ in lymphatic endothelium, or *C*, in the presence of 2 mM $[Ca^{2+}]_o$ and during virtual blockade of TRPV4 and Orai channels. Note that removal of the Ca^{2+} from outside or blockade of membrane Ca^{2+} channels in the model also results in an abolished plateau phase (compare to Fig. 4*A* and *B*). *D*, V_m during ACh for lymphatic endothelium showing the depolarization similar to experimental recordings (Fig. 2*F*). *E*, as in *D*, with V_m calculated during ACh in the absence of $[Ca^{2+}]_o$, or *F*, in the presence of 2 mM $[Ca^{2+}]_o$ and during virtual blockade of TRPV4 and Orai channels (compare to Fig. 4*C* and *D*). Note that depolarization is abolished only with $LaCl_3$ and not in the absence of $[Ca^{2+}]_o$, suggesting a role for Na^+ currents in depolarization.

in striking contrast to the hyperpolarization of blood vessel endothelium attributable to the efflux of K^+, we find that the rise in $[Ca^{2+}]_i$ in LECs is associated with depolarization attributable to the influx of Ca^{2+} and Na^+. The depolarization observed in LEC tubes in response to ACh was confirmed in intact collecting lymphatic vessels that were pressurized and contracting. Moreover, the absence of SK_{Ca}/IK_{Ca} activity and gene expression in LECs is in contrast to the robust expression of these channels in arterial endothelium (Jackson, 2005; Ledoux *et al.* 2006; Behringer & Segal, 2012). Whereas sustained elevation of $[Ca^{2+}]_i$ was abolished by removing extracellular Ca^{2+} or blocking the entry of Ca^{2+} through TRPV4, depolarization persisted until Na^+ was prevented from entering cells through non-selective cation channels with $LaCl_3$. These findings build on previous electrophysiological studies of LECs in guinea pig mesenteric lymphatic vessels (von der Weid & Van Helden, 1997).

Physiological relevance

The EDH response in arterial endothelium is associated with hyperpolarization through activation of SK_{Ca}/IK_{Ca}

channels, which is then conducted along the endothelial layer via homocellular gap junctions and into surrounding SMCs through myoendothelial gap junctions to coordinate dilatation along the vessel (Bagher & Segal, 2011, Garland *et al.* 2011). In the present study, our data suggest that LECs lack SK_{Ca}/IK_{Ca} channels responsible for EDH. Taken together with our previous findings that popliteal collecting lymphatic vessel dilatation to ACh is blocked completely by inhibiting NO production (Scallan & Davis, 2013), it appears that muscular lymphatic vessels do not possess an EDH pathway. Further, it appears likely that mouse lymphatic endothelium does not exhibit conducted hyperpolarization, given that its resting V_m of ~-70 mV is already quite negative as shown here in both LECTs and in intact lymphatic endothelium, which is in agreement with a previous report (von der Weid & Van Helden, 1997). Thus, LECs are poised to depolarize rather than hyperpolarize and depolarization would attenuate the driving force for Ca^{2+} entry and subsequent NO production through eNOS. This interpretation is consistent with LEC depolarization serving to permit LMC contraction.

ECs and SMCs of blood vessels are coupled electrically (Emerson & Segal, 2000), but there is so far a lack of
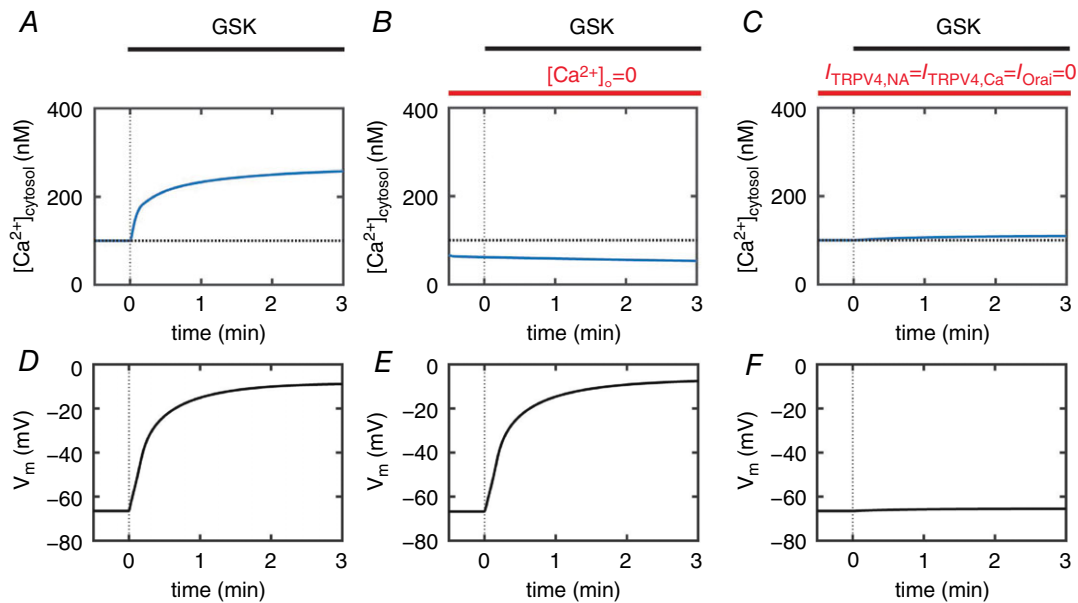

Figure 9. Computational modelling: intracellular Ca^{2+} changes with V_m during continuous stimulation with GSK101

A, $[Ca^{2+}]_i$ changes during GSK101 (with 2 mM $[Ca^{2+}]_o$) in lymphatic endothelium. Opening TRPV4 channels leads to an increase in $[Ca^{2+}]_i$ similar to that observed in Fura-2 experiments (Fig. 5*A*). *B*, as in *A*, in the absence of $[Ca^{2+}]_o$ in lymphatic endothelium, or *C*, in the presence of 2 mM $[Ca^{2+}]_o$ and during virtual blockade of TRPV4 and Orai channels. Note that removal of external Ca^{2+} or blockade of membrane Ca^{2+} channels in the model abolished any change in $[Ca^{2+}]_i$ (compare to Fig. 5*B* and *C*). *D*, V_m during GSK (with 2 mM $[Ca^{2+}]_o$) for lymphatic endothelium showing depolarization similar to experimental recording (Fig. 5*D*). *E*, as in *D*, calculated V_m during GSK101 in the absence of $[Ca^{2+}]_o$ in lymphatic endothelium, or *F*, in the presence of 2 mM $[Ca^{2+}]_o$ and during virtual blockade of TRPV4 and Orai channels. Note that depolarization is present in *E* (GSK + 0 $[Ca^{2+}]_o$) but not in *F* (GSK + $LaCl_3$) similar to the experimental recording (compare to Fig. 5*E* and *F*). Further, note similarities in *C* and *F* compared to Fig. 5*C* and *F*, respectively, consistent with recordings obtained from LECTs of *Trpv4*$^{-/-}$ mice.

evidence that LECs and LMCs are coupled to each other in this manner. In fact, because these two cell layers differ in their respective V_m at rest (LMCs: −45 mV and LECs: −70 mV), there must be a barrier to the passage of substantial electrical charge between them (von der Weid & Van Helden, 1997), despite the fact that LECs are known to express several connexin isoforms, including Cx43 and Cx37 (Kanady *et al.* 2011; Sabine *et al.* 2012; Munger *et al.* 2016). The lack of electrical current passage between the LECs and LMCs was confirmed in the present study by recording a stable lymphatic endothelial membrane potential in intact lymphatic vessels that were contracting, and thus were coated with smooth muscle cells that were firing repetitive action potentials. One outcome from this lack of direct coupling is that the lymphatic endothelium is unable to regulate LMC contraction through electrical signals. The lack of coupling between respective cell layers would prevent loss of charge from LMCs into LECs, thereby facilitating conduction of

a contraction wave (i.e. depolarization) along the LMC layer. Therefore, we propose that collecting lymphatic vessels are optimized for the initiation and conduction of depolarization, in contrast to blood vascular endothelium, which is optimized for the initiation and conduction of hyperpolarization signals that drive vasodilatation.

TRPV4 currents predominate in lymphatic endothelium

Previous studies have established a role for TRPV4 channels in promoting Ca^{2+} influx into the endothelium of resistance arteries, whereby activation of SK_{Ca}/IK_{Ca} and hyperpolarization produces vasodilatation (Zhang *et al.* 2009; Sonkusare *et al.* 2012; Qian *et al.* 2014). In the present study, mice genetically lacking *Trpv4* show a ∼70% reduction in depolarization to ACh during the plateau phase as compared to wild-type C57BL/6 mice (see Fig. 6*E*, right panel). To our knowledge, this is the first study to
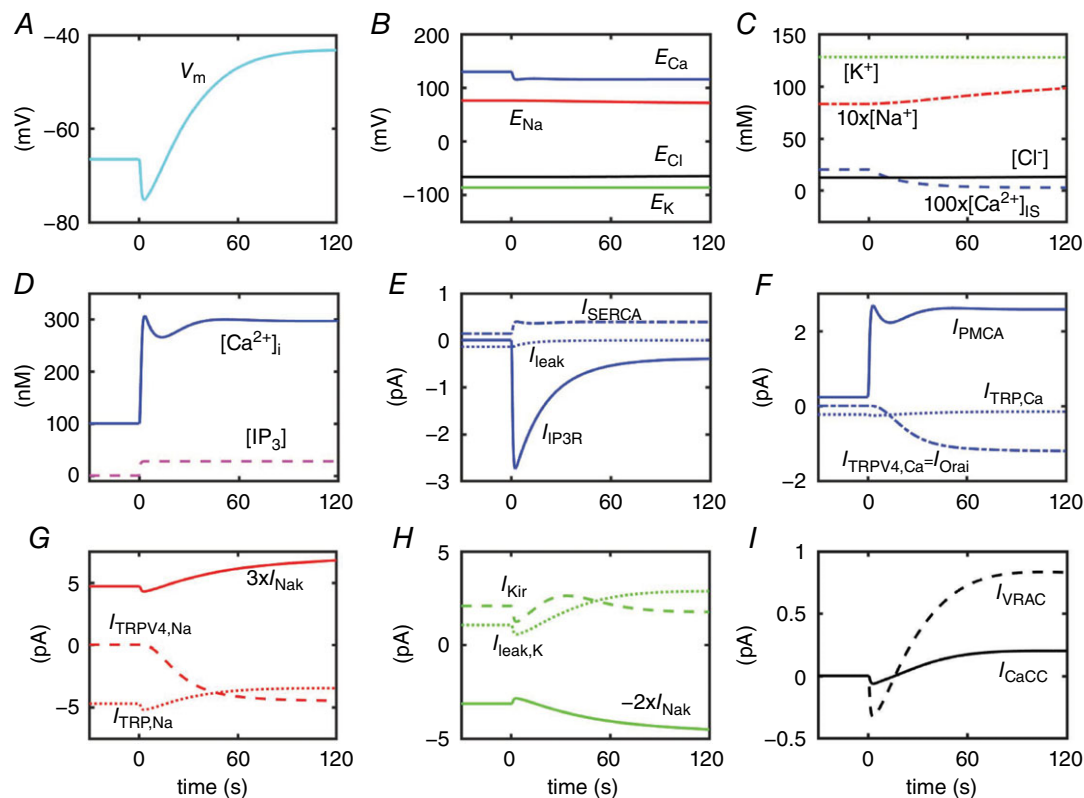

Figure 10. Computational modelling: dynamics in ionic fluxes and open probability of key channels, exchangers, and pumps
A, V_m under baseline conditions (time < 0 s) and during ACh (starting at time 0 s). *B*, as in *A* for the equilibrium potential for Ca^{2+} (E_{Ca}), equilibrium potential for Na^+ (E_{Na}), equilibrium potential for K^+ (E_K) and equilibrium potential for Cl^- (E_{Cl}). *C*, for $[K^+]$, $[Na^+]$, $[Cl^-]$ and $[Ca^{2+}]_{IS}$. *D*, for $[Ca^{2+}]_i$ and $[IP_3]_i$. *E*, for I_{IP3R}, I_{SERCA} and I_{leak}. *F*, I_{PMCA}, $I_{TRP,Ca}$, $I_{TRPV4,Ca}$ and I_{Orai}. *G*, for $3 \times I_{NaK}$, $I_{TRP,Na}$, $I_{TRPV4,Na}$. *H*, for $-2 \times I_{NaK}$ (negative sign is to account for inward K^+ current by NaK), I_{Kir} and $I_{leak,K}$. *I*, for I_{CaCC} and I_{VRAC}. In *C*, $[Na^+]$ is plotted multiplied by a factor of 10, and $[Ca^{2+}]_{IS}$ by a factor of 100 for visualization. Note that negative currents are inward and positive currents are outward. V_m is shown in cyan and $[IP_3]$ is in magenta while concentration and currents for K^+ are in green, Na^+ are in red, Cl^- are in black and Ca^{2+} are in blue. For direct comparison, this figure contains similar types of data to Fig. 7 from Silva *et al.* (2007), which shows the model for mesenteric artery endothelium in response to ACh.

indicate a functional role for TRPV4 in governing cation influx in lymphatic endothelium. The robust entry of Ca^{2+} and Na^+ combined with a lack of SK_{Ca}/IK_{Ca} channel activity results in an accumulation of positive charge along the intracellular side of the plasma membrane, thereby leading to depolarization of V_m (Hille, 2001) (Fig. 2). As the absence of extracellular Ca^{2+} reduced depolarization by nearly half during ACh stimulation (Fig. 4E, right panel), our findings suggest an equal role for Na^+ entry in depolarizing LECs. Furthermore, as the direct activation of TRPV4 channels with GSK101 elicits a full depolarization response in the absence of $[Ca^{2+}]_o$ (Figs 5 and 9), the influx of Na^+ alone can fulfil this physiological role of TRPV4 in membrane depolarization during the regulation of lymphatic function. Consistent with this interpretation is that blocking non-selective cation channels with $LaCl_3$ (Fig. 5F and H) or genetic deletion of *Trpv4* (Fig. 6D and F, right panel) eliminated depolarization to GSK101.

Mathematical modelling analysis

The mathematical model presented here is based on a well-developed model of mesenteric artery endothelium (Silva *et al.* 2007) that could reproduce our experimental measurement of $[Ca^{2+}]_i$ and V_m in mouse popliteal arteries (Fig. 2C and E). Removal of the SK_{Ca}/IK_{Ca} currents was based on the present experiments in which blocking agents were applied without significant effects (Fig. 1) and the lack of LECT hyperpolarization to either ACh or GSK. With approximation of the model parameters to reflect the more negative V_m in LECs compared to vascular ECs, we matched $[Ca^{2+}]_i$ and V_m dynamics to our experimental data for ACh and GSK (compare Figs 4 and 5 to Figs 8 and 9). To further substantiate our application of this model to LECs, we compared the results from blocking ion channels and found a similar degree of depolarization after K_{ir} blockade (~11.3 mV computationally *versus* 11 ± 1 mV experimentally). Additionally, NaK blockade in guinea pig lymphatic endothelium with ouabain (von der Weid & Van Helden, 1997) produced a 6 mV depolarization, similar to the predictions of our model (6.7 mV). In a previous *in vitro* study of cultured LECs with Fura-2 measurement of $[Ca^{2+}]_i$, the SERCA inhibitor thapsigargin elicited rapid ER depletion followed by a sustained $[Ca^{2+}]_i$ increase from TRPV4 and Orai activation (Jafarnejad *et al.* 2015). We observed a similar dynamic in our model when SERCA current was removed. We conclude that our model of LECs demonstrates the details of ionic current balance in the resting condition as well as during ACh treatment and can therefore be utilized to generate novel hypotheses by investigating scenarios that include blockade of ion channels for which selective pharmacological tools are lacking. First, the model predicts that PMCA channels are required for Ca^{2+} extrusion after stimulation

with ACh and therefore their blockade would lead to a considerable increase in $[Ca^{2+}]_i$, a point that should be investigated experimentally (Fig. 10F). Second, the model predicts that the Na^+ permeability of TRPV4 channels is essential for ACh-mediated depolarization of LECTs, which is consistent with the central finding of the present experiments. Third, the model identifies the $Ca^{2+}:Na^+$ permeability ratio of TRPV4 as a primary parameter in determining the balance between sustained influx of Ca^{2+} *versus* V_m depolarization. Fourth, it predicts that after ACh stimulation, 56% of the total Na^+ TRP current is through TRPV4, which is in agreement with arteriolar endothelium (Sonkusare *et al.* 2012). Overall, the model provides a comprehensive picture of all requisite transmembrane currents, ionic concentrations, and potentials, which are otherwise difficult or impractical to measure experimentally. For instance, the model offers a tantalizing prediction as to why the resting V_m is significantly more negative in lymphatic endothelium *versus* blood endothelium: the potential absence of significant NKCC channel expression would prevent the inward Cl^- current that underlies the steady-state depolarization in blood endothelium (Russell, 2000).

Summary and conclusions

The function of endothelial Ca^{2+}-activated K^+ channels as an interface between intracellular Ca^{2+} dynamics and production of hyperpolarization has long been recognized (Busse *et al.* 1988). An integral component of resistance blood vessels is to coordinate smooth muscle cell relaxation and vasodilatation in accord with metabolic demand (Segal, 2015). Conversely, collecting lymphatics also undergo active Ca^{2+} and electrical dynamics (von der Weid & Van Helden, 1997; Ferrusi *et al.* 2004) but do so to generate rhythmic contractions and unidirectional pumping of fluid (von der Weid *et al.* 1996; Mizuno *et al.* 1997). We sought to resolve the underlying ionic mechanisms of lymphatic endothelial function working from our established understanding of endothelium-derived hyperpolarization demonstrated in blood vessel endothelium. Overall, we found that while $[Ca^{2+}]_i$ dynamics were similar to arterial endothelium in response to agonists such as ACh, depolarization (rather than hyperpolarization) ensued in lymphatic endothelium. This striking difference can be explained by the lack of Ca^{2+}-activated K^+ channels in LECs while Ca^{2+} and Na^+ ions enter through non-selective TRPV4 cation channels. Thus, the lack of an EDH pathway in lymphatic endothelium is likely a crucial adaptation to ensure the efficient conduction of contraction waves in the adjacent lymphatic muscle cells that are required for propulsive lymph flow.

References

Aspelund A, Robciuc MR, Karaman S, Makinen T & Alitalo K (2016). Lymphatic system in cardiovascular medicine. *Circ Res* **118**, 515–530.

Bagher P & Segal SS (2011). Regulation of blood flow in the microcirculation: role of conducted vasodilation. *Acta Physiol (Oxf)* **202**, 271–284.

Behringer EJ & Segal SS (2012). Tuning electrical conduction along endothelial tubes of resistance arteries through Ca^{2+}-activated K^+ channels. *Circ Res* **110**, 1311–1321.

Behringer EJ & Segal SS (2015). Membrane potential governs calcium influx into microvascular endothelium: integral role for muscarinic receptor activation. *J Physiol* **593**, 4531–4548.

Behringer EJ, Socha MJ, Polo-Parada L & Segal SS (2012). Electrical conduction along endothelial cell tubes from mouse feed arteries: confounding actions of glycyrrhetinic acid derivatives. *Br J Pharmacol* **166**, 774–787.

Busse R, Edwards G, Félétou M, Fleming I, Vanhoutte PM & Weston AH (2002). EDHF: bringing the concepts together. *Trends Pharmacol Sci* **23**, 374–380.

Busse R, Fichtner H, Luckhoff A & Kohlhardt M (1988). Hyperpolarization and increased free calcium in acetylcholine-stimulated endothelial cells. *Am J Physiol Heart Circ Physiol* **255**, H965–H969.

Chakraborty S, Davis MJ & Muthuchamy M (2015). Emerging trends in the pathophysiology of lymphatic contractile function. *Semin Cell Dev Biol* **38**, 55–66.

Choi D, Park E, Jung E, Seong YJ, Hong M, Lee S, Burford J, Gyarmati G, Peti-Peterdi J, Srikanth S, Gwack Y, Koh CJ, Boriushkin E, Hamik A, Wong AK & Hong YK (2017*a*). ORAI1 activates proliferation of lymphatic endothelial cells in response to laminar flow through Kruppel-like factors 2 and 4. *Circ Res* **120**, 1426–1439.

Choi D, Park E, Jung E, Seong YJ, Yoo J, Lee E, Hong M, Lee S, Ishida H, Burford J, Peti-Peterdi J, Adams RH, Srikanth S, Gwack Y, Chen CS, Vogel HJ, Koh CJ, Wong AK & Hong YK (2017*b*). Laminar flow downregulates Notch activity to promote lymphatic sprouting. *J Clin Invest* **127**, 1225–1240.

Clapham DE, Julius D, Montell C & Schultz G (2005). International Union of Pharmacology. XLIX. Nomenclature and structure-function relationships of transient receptor potential channels. *Pharmacol Rev* **57**, 427–450.

Cohen KD & Jackson WF (2005). Membrane hyperpolarization is not required for sustained muscarinic agonist-induced increases in intracellular Ca^{2+} in arteriolar endothelial cells. *Microcirculation* **12**, 169–182.

Davis MJ, Scallan JP, Wolpers JH, Muthuchamy M, Gashev AA & Zawieja DC (2012). Intrinsic increase in lymphangion muscle contractility in response to elevated afterload. *Am J Physiol Heart Circ Physiol* **303**, H795–H808.

Diep HK, Vigmond EJ, Segal SS & Welsh DG (2005). Defining electrical communication in skeletal muscle resistance arteries: a computational approach. *J Physiol* **568**, 267–281.

Emerson GG, Neild TO & Segal SS (2002). Conduction of hyperpolarization along hamster feed arteries: augmentation by acetylcholine. *Am J Physiol Heart Circ Physiol* **283**, H102–H109.

Emerson GG & Segal SS (2000). Electrical coupling between endothelial cells and smooth muscle cells in hamster feed arteries: role in vasomotor control. *Circ Res* **87**, 474–479.

Félétou M (2016). Endothelium-dependent hyperpolarization and endothelial dysfunction. *J Cardiovasc Pharmacol* **67**, 373–387.

Ferrusi I, Zhao J, van Helden D & von der Weid PY (2004). Cyclopiazonic acid decreases spontaneous transient depolarizations in guinea pig mesenteric lymphatic vessels in endothelium-dependent and -independent manners. *Am J Physiol Heart Circ Physiol* **286**, H2287–H2295.

Fill M & Copello JA (2002). Ryanodine receptor calcium release channels. *Physiol Rev* **82**, 893–922.

Garland CJ & Dora KA (2017). EDH: endothelium-dependent hyperpolarization and microvascular signaling. *Acta Physiol (Oxf)* **219**, 152–161.

Garland CJ, Hiley CR & Dora KA (2011). EDHF: spreading the influence of the endothelium. *Br J Pharmacol* **164**, 839–852.

Gees M, Colsoul B & Nilius B (2010). The role of transient receptor potential cation channels in Ca^{2+} signaling. *Cold Spring Harb Perspect Biol* **2**, a003962.

Hald BO, Welsh DG, Holstein-Rathlou NH & Jacobsen JC (2015). Origins of variation in conducted vasomotor responses. *Pflugers Arch* **467**, 2055–2067.

Hill-Eubanks DC, Gonzales AL, Sonkusare SK & Nelson MT (2014). Vascular TRP channels: performing under pressure and going with the flow. *Physiology (Bethesda)* **29**, 343–360.

Hille B (2001). *Ion Channels of Excitable Membranes*, 3rd edn, Ch. 22, Evolution and origins, pp. 693–722. Sinauer Associates, Sunderland.

Himmel HM, Whorton AR & Strauss HC (1993). Intracellular calcium, currents, and stimulus-response coupling in endothelial cells. *Hypertension* **21**, 112–127.

Jackson WF (2005). Potassium channels in the peripheral microcirculation. *Microcirculation* **12**, 113–127.

Jafarnejad M, Cromer WE, Kaunas RR, Zhang SL, Zawieja DC & Moore JE Jr (2015). Measurement of shear stress-mediated intracellular calcium dynamics in human dermal lymphatic endothelial cells. *Am J Physiol Heart Circ Physiol* **308**, H697–H706.

Kanady JD, Dellinger MT, Munger SJ, Witte MH & Simon AM (2011). Connexin37 and Connexin43 deficiencies in mice disrupt lymphatic valve development and result in lymphatic disorders including lymphedema and chylothorax. *Dev Biol* **354**, 253–266.

Koenigsberger M, Sauser R, Beny JL & Meister JJ (2005). Role of the endothelium on arterial vasomotion. *Biophys J* **88**, 3845–3854.

Ledoux J, Werner ME, Brayden JE & Nelson MT (2006). Calcium-activated potassium channels and the regulation of vascular tone. *Physiology (Bethesda)* **21**, 69–78.

Liao Y, Erxleben C, Abramowitz J, Flockerzi V, Zhu MX, Armstrong DL & Birnbaumer L (2008). Functional interactions among Orai1, TRPCs, and STIM1 suggest a STIM-regulated heteromeric Orai/TRPC model for SOCE/Icrac channels. *Proc Natl Acad Sci USA* **105**, 2895–2900.

Lindblad DS, Murphey CR, Clark JW & Giles WR (1996). A model of the action potential and underlying membrane currents in a rabbit atrial cell. *Am J Physiol Heart Circ Physiol* **271**, H1666–H1696.

Ma X, Cheng K-T, Wong C-O, O'Neil RG, Birnbaumer L, Ambudkar IS & Yao X (2011). Heteromeric TRPV4-C1 channels contribute to store-operated Ca^{2+} entry in vascular endothelial cells. *Cell Calcium* **50**, 502–509.

Mizuno R, Dornyei G, Koller A & Kaley G (1997). Myogenic responses of isolated lymphatics: modulation by endothelium. *Microcirculation* **4**, 413–420.

Munger SJ, Geng X, Srinivasan RS, Witte MH, Paul DL & Simon AM (2016). Segregated Foxc2, NFATc1 and connexin expression at normal developing venous valves, and connexin-specific differences in the valve phenotypes of Cx37, Cx43, and Cx47 knockout mice. *Dev Biol* **412**, 173–190.

Prins D & Michalak M (2011). Organellar calcium buffers. *Cold Spring Harb Perspect Biol* **3**, a004069.

Qian X, Francis M, Kohler R, Solodushko V, Lin M & Taylor MS (2014). Positive feedback regulation of agonist-stimulated endothelial Ca^{2+} dynamics by $K_{Ca}3.1$ channels in mouse mesenteric arteries. *Arterioscler Thromb Vasc Biol* **34**, 127–135.

Ruhle B & Trebak M (2013). Emerging roles for native Orai Ca^{2+} channels in cardiovascular disease. *Curr Top Membr* **71**, 209–235.

Russell JM (2000). Sodium-potassium-chloride cotransport. *Physiol Rev* **80**, 211–276.

Sabine A, Agalarov Y, Maby-El Hajjami H, Jaquet M, Hagerling R, Pollmann C, Bebber D, Pfenniger A, Miura N, Dormond O, Calmes JM, Adams RH, Makinen T, Kiefer F, Kwak BR & Petrova TV (2012). Mechanotransduction, PROX1, and FOXC2 cooperate to control connexin37 and calcineurin during lymphatic-valve formation. *Dev Cell* **22**, 430–445.

Scallan JP & Davis MJ (2013). Genetic removal of basal nitric oxide enhances contractile activity in isolated murine collecting lymphatic vessels. *J Physiol* **591**, 2139–2156.

Scallan JP, Wolpers JH & Davis MJ (2013). Constriction of isolated collecting lymphatic vessels in response to acute increases in downstream pressure. *J Physiol* **591**, 443–459.

Segal SS (2015). Integration and modulation of intercellular signaling underlying blood flow control. *J Vasc Res* **52**, 136–157.

Silva HS, Kapela A & Tsoukias NM (2007). A mathematical model of plasma membrane electrophysiology and calcium dynamics in vascular endothelial cells. *Am J Physiol Cell Physiol* **293**, C277–C293.

Socha MJ, Domeier TL, Behringer EJ & Segal SS (2012). Coordination of intercellular Ca^{2+} signaling in endothelial cell tubes of mouse resistance arteries. *Microcirculation* **19**, 757–770.

Socha MJ, Hakim CH, Jackson WF & Segal SS (2011). Temperature effects on morphological integrity and Ca^{2+} signaling in freshly isolated murine feed artery endothelial cell tubes. *Am J Physiol Heart Circ Physiol* **301**, H773–H783.

Socha MJ & Segal SS (2013). Isolation of microvascular endothelial tubes from mouse resistance arteries. *J Vis Exp* **81**, e50759.

Sonkusare SK, Bonev AD, Ledoux J, Liedtke W, Kotlikoff MI, Heppner TJ, Hill-Eubanks DC & Nelson MT (2012). Elementary Ca^{2+} signals through endothelial TRPV4 channels regulate vascular function. *Science* **336**, 597–601.

Sonkusare SK, Dalsgaard T, Bonev AD, Hill-Eubanks DC, Kotlikoff MI, Scott JD, Santana LF & Nelson MT (2014). AKAP150-dependent cooperative TRPV4 channel gating is central to endothelium-dependent vasodilation and is disrupted in hypertension. *Sci Signal* **7**, ra66.

Thorneloe KS, Sulpizio AC, Lin Z, Figueroa DJ, Clouse AK, McCafferty GP, Chendrimada TP, Lashinger ES, Gordon E, Evans L, Misajet BA, Demarini DJ, Nation JH, Casillas LN, Marquis RW, Votta BJ, Sheardown SA, Xu X, Brooks DP, Laping NJ & Westfall TD (2008). N-((1S)-1-{[4-((2S)-2-{[(2,4-dichlorophenyl)sulfonyl]amino}-3-hydroxypropanoyl)-1-piperazinyl]carbonyl}-3-methyl butyl)-1-benzothiophene-2-carboxamide (GSK1016790A), a novel and potent transient receptor potential vanilloid 4 channel agonist induces urinary bladder contraction and hyperactivity: Part I. *J Pharmacol Exp Ther* **326**, 432–442.

Voets T, Droogmans G, Raskin G, Eggermont J & Nilius B (1999). Reduced intracellular ionic strength as the initial trigger for activation of endothelial volume-regulated anion channels. *Proc Natl Acad Sci USA* **96**, 5298–5303.

von der Weid PY, Crowe MJ & Van Helden DF (1996). Endothelium-dependent modulation of pacemaking in lymphatic vessels of the guinea-pig mesentery. *J Physiol* **493**, 563–575.

von der Weid PY, Lee S, Imtiaz MS, Zawieja DC & Davis MJ (2014). Electrophysiological properties of rat mesenteric lymphatic vessels and their regulation by stretch. *Lymphat Res Biol* **12**, 66–75.

von der Weid PY & Van Helden DF (1997). Functional electrical properties of the endothelium in lymphatic vessels of the guinea-pig mesentery. *J Physiol* **504**, 439–451.

Wiesner TF, Berk BC & Nerem RM (1996). A mathematical model of cytosolic calcium dynamics in human umbilical vein endothelial cells. *Am J Physiol Cell Physiol* **270**, C1556–C1569.

Yang J, Clark JW Jr, Bryan RM & Robertson C (2003). The myogenic response in isolated rat cerebrovascular arteries: smooth muscle cell model. *Med Eng Physics* **25**, 691–709.

Zhang DX, Mendoza SA, Bubolz AH, Mizuno A, Ge ZD, Li R, Warltier DC, Suzuki M & Gutterman DD (2009). Transient receptor potential vanilloid type 4-deficient mice exhibit impaired endothelium-dependent relaxation induced by acetylcholine in vitro and in vivo. *Hypertension* **53**, 532–538.

Additional information

Competing interests

The authors have no competing interests to declare or conflicts of interest to disclose. The content of this article is solely the responsibility of the authors and does not necessarily represent the official views of the National Institutes of Health.

Author contributions

E.J.B., J.P.S., J.A.C. and S.D.Z. designed and performed experiments in the laboratories of S.S.S. and M.J.D. M.J.

performed computational modelling in the laboratory of J.E.M. E.J.B., J.P.S., M.J.D., J.A.C., S.D.Z. and S.S.S. analysed and interpreted data. E.J.B., J.P.S., M.J., S.D.Z. and J.A.C. drafted the manuscript and/or prepared the figures. S.S.S. and M.J.D. edited the manuscript. All authors approved the final version of the manuscript and agree to be accountable for all aspects of the work in ensuring that questions related to the accuracy or integrity of any part of the work are appropriately investigated and resolved. All persons designated as authors qualify for authorship, and all those who qualify for authorship are listed.

Translational perspective

In the blood circulation, endothelial cell function in resistance vessels employs activation of Ca^{2+}-sensitive K^+ channels to hyperpolarize and promote relaxation of vascular smooth muscle cells. Thus, vasodilatation can be triggered through TRPV4 channels that promote Ca^{2+} influx. However, in the lymphatic circulation it is unknown whether the endothelium uses Ca^{2+}-sensitive K^+ channel activity to govern the activity of lymphatic muscle cells for pumping fluid away from peripheral tissues to prevent oedema. To answer this question, we studied freshly isolated endothelial tubes of collecting lymphatic vessels that are free of such confounding factors as smooth muscle cells and the flow of lymph. We evaluated intracellular Ca^{2+} levels in conjunction with membrane potential during exposure to pharmacological agents known to activate Ca^{2+}-sensitive K^+ channels and TRPV4 channels to elevate intracellular Ca^{2+}. Our findings indicate that, despite robust increases in intracellular Ca^{2+}, the endothelium of collecting lymphatics lacks Ca^{2+}-sensitive K^+ channels yet expresses TRPV4 channels and depolarizes with Ca^{2+} influx. Genetic deletion of *Trpv4* attenuated Ca^{2+} influx, confirming the integral role of TRPV4 channels in lymphatic endothelium. Our findings indicate that (1) endothelial Ca^{2+}-sensitive K^+ channel activity is not requisite for lymphatic function and (2) vascular endothelia throughout the body need not share the same genetic and protein composition to perform their physiological roles. These data provide fundamentally new insight for precision medicine, whereby selective treatments are developed for key vascular biomarkers to promote health and cure disease.